

LISA: A Modern Astrophysical Observatory

Shane L. Larson

Center for Gravitational Wave Physics, The Pennsylvania State University, University Park, PA 16802

The Laser Interferometer Space Antenna (LISA) is a spaceborne gravitational wave observatory which will be sensitive to low-frequency gravitational waves in the frequency range from about 100 microHertz up to about 1 Hz. The mission is being jointly pursued by NASA and the European Space Agency (ESA), and at the time of this writing¹ is slated for a launch in 2014. Comprised of a constellation of three free-flying spacecraft, LISA will be sensitive to supermassive black hole binaries, close interacting binaries in the galaxy, the capture of stellar mass objects by supermassive black holes in galactic nuclei, and possibly to stochastic backgrounds of gravitational radiation of cosmological origin. This review summarizes in brief the current description of the LISA observatory, how it will function as an interferometer, the sensitivity it will have to sources of gravitational radiation, and a simple taxonomy of prospective astrophysical sources. It also provides simple pocket formulae which are often useful for making computations about sources in the LISA band.

1. INTRODUCTION

In observational astronomy, different facilities and instrumentation are needed to probe different parts of the electromagnetic spectrum. Gravitational wave astronomy is similar in this respect. Ground based interferometric observatories like LIGO [1], GEO600 [2] and VIRGO [3] provide broadband coverage of the gravitational wave spectrum at frequencies ranging from a few Hz to a few kHz. Narrow-band resonant bar detectors [4, 5] probe narrow parts of the high frequency spectrum at hundreds of Hz. At frequencies below a few Hz, natural sources of noise associated with the seismic activity of the Earth precludes the possibility of a ground-based observatory designed to probe the low-frequency gravitational wave spectrum; furthermore, the wavelengths of the gravitational waves of interest also rapidly become too large to capture, even with a detector which could span the entire globe. To probe the low-frequency part of the gravitational wave spectrum, at frequencies below 1 Hz down to tens of microHertz, it is necessary to build detectors in space. At extremely low frequencies, below a microhertz, detection is only possible through Doppler tracking of interplanetary spacecraft [6–8], accurate timing of pulsars [9, 10] and polarization effects in the Cosmic Microwave Background [11].

The fact that spaceborne observatories would be needed to probe the low-frequency spectrum was known early on, with early reviews on the subject simply referring to such detectors as “beams in space” (see, *e.g.*, [12]). Early studies were instigated at the Joint Institute for Laboratory Astrophysics (JILA) in the early 1980s, and in 1985 the first full description of a spaceborne gravitational-wave observatory was put forward in the form of LAGOS (Laser Antenna for Gravitational-radiation Observation in Space) [13]. Other spaceborne designs followed, notably ecliptic plane interferometers such as SAGITTARIUS (Spaceborne Astronomical Gravitational-wave Interferometer To Test Aspects of Relativity and Investigate Unknown Sources) [14] and OMEGA (Orbiting Medium Explorer for Gravitational-wave Astrophysics) [15]. LISA as a mission first appeared in 1993 as a mission proposal to ESA’s *Horizon 2000* program, for which LISA ultimately became a cornerstone project. By 1997, LISA had become a joint project between NASA and ESA, with mission characterization and design efforts being carried out on both sides of the Atlantic.

Gravitational wave astronomy, and LISA in particular, were recognized as national research priorities in the most recent decadal surveys [16, 17]. Currently, LISA is one of NASA’s two “Einstein Observatories”, which are the flagship missions underpinning the *Beyond Einstein* program [18]; the other mission is an a constellation of free flying x-ray telescopes known as *Constellation-X* [19]. The division of responsibility for the LISA mission is expected

¹Fall, 2005

to be split more or less evenly between NASA and the European Space Agency.

LISA is currently in what is known as the *formulation* phase (“Phase A”), where the science requirements are fixed and the mission requirements, as a consequence, are set. The next phase (so-called *implementation*, “Phase B”) will begin near the end of the decade, leading to a launch in approximately 2014. In the interim, a technology precursor mission known as *LISA Pathfinder* is scheduled to launch in the 2006 – 2007 timeframe. Like LISA, *Pathfinder* will be a joint enterprise between NASA and ESA, and is designed to test the core disturbance reduction sensor technology which will be at the heart of a single LISA spacecraft. The goal of the *Pathfinder* mission is to reach an acceleration noise level which is within about 1 order of magnitude of the LISA mission requirements.

This paper summarizes some of the key aspects of current research which play a vital role in the design and characterization of the LISA mission. An effort has been made to divide the discussion more or less evenly between issues related to the technology and design of the LISA mission, and the science and astrophysics which will be enabled by the observatory. The intent is to provide as broad a view as possible of the current research related to the mission, at the expense of providing full details (interested readers should peruse the referenced literature for more extensive discussions). As a review of LISA, this document is by no means complete nor exhaustive in its overview of the literature. It is intended only to provide brief introductions to relevant science and technical issues associated with the LISA mission and to provide contact points with the literature in these areas, thus allowing the interested person to begin their own scholarly endeavours in this field. Where appropriate, more extensive reviews on a particular topic have been noted.

The rest of this paper is organized as follows. Section 2 looks at the design and technology of the observatory, including details about the spacecraft and constellation (§ 2.1), time delay interferometry (§ 2.2), and interferometry applications (§ 2.3). Section 3 discusses how LISA will operate as an observatory, examining how to compute representations of the observatory’s sensitivity (§ 3.1), some pocket formulae useful for making estimates related to gravitational wave emission from compact binary systems (§ 4.2), and an examination of the different ways the strength of sources are represented in the LISA literature (§ 3.3). Section 4 considers the science that can be done with LISA; it begins with the key science drivers for the mission (§ 4.1). The rest of the section is dedicated to the basic classes of sources LISA is expected to observe, including the galactic population of close binaries (§ 4.2), supermassive black hole binaries (§ 4.3), and extreme mass ratio inspirals (§ 4.4). The section concludes with discussion of LISA probes of fundamental physics (§ 4.5), and a brief mention of other possible, though likely rare, source detections in the LISA band (§ 4.6). A short summary concludes this review (§5).

Unless otherwise noted, geometrized units are used throughout, where $G = c = 1$. In these units time, mass and energy are measured in units of length. Conventional units will generally be restored when discussing observable astrophysical quantities.

2. THE LISA MISSION

LISA is an evolving mission, and has not yet had its design frozen as part of the build-up to construction and launch. Its character has been relatively static for some time now, and has been extensively described in two large technical documents known as the *LISA Pre-Phase A Report* (LPPA) [20] produced by the LISA Study Team, and the *Final Technical Report* (FTR) [21] produced by a European alliance of industry and academic partners interested in LISA. Another summary of the project is the *System and Technology Study Report* (STS) [22], written as part of the plan to make LISA a collaborative enterprise between NASA and ESA.

The description of the mission discussed here will follow these “official” documents; when necessary to follow a particular convention or description, those outlined in the LPPA are used. The base parameters describing the design of the observatory are noted in Table I.

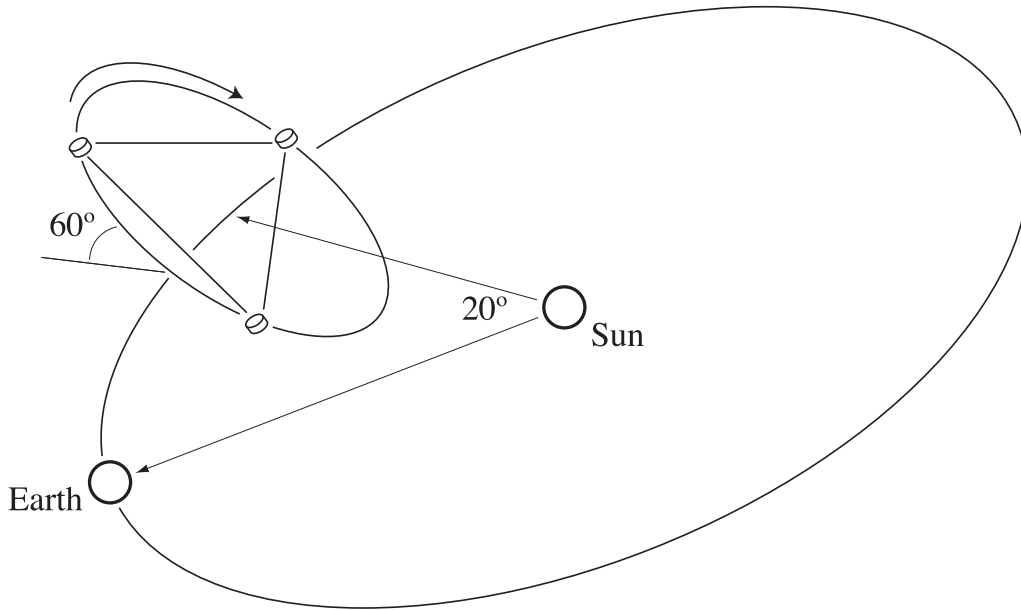


Figure 1: The final orbital configuration of LISA. The *guiding center* of the constellation orbits on the ecliptic at a distance of 1 AU from the Sun, trailing 20° behind the Earth. The constellation plane is inclined by 60° to the ecliptic, and as viewed from the Sun, appears to rotate in a clockwise direction, reverse cartwheeling as the observatory orbits the Sun.

2.1. Spacecraft Constellation

The complete LISA observatory is comprised of three spacecraft, free flying and arranged in an approximately equilateral triangle, each spacecraft exchanging laser signals through its telescopes with the two adjacent spacecraft. The separation between any two spacecraft in the constellation is $L_o = 5 \times 10^9$ m, yielding laser propagation times of $\tau = 16.68$ s down each arm.

As a single entity, the constellation of three spacecraft appears to move together around the Sun, centered on a point known as the *guiding center*. The guiding center lies on the Earth orbit, trailing 20° ($\sim 5.2 \times 10^7$ km) behind the planet. As viewed from the Sun, the constellation appears to rotate *clockwise* around the guiding center, in a so-called “reverse cartwheel” motion. The constellation orbit and configuration is shown in Figure 1.

While this seemingly complicated motion may appear difficult to describe, it is simply a consequence of the relative motion of each of the individual spacecraft on standard elliptical, Keplerian orbits with semi-major axis approximately the same as the Earth’s orbital radius, R_\oplus , eccentricities of $e = L_o / (2\sqrt{3}R_\oplus)$ and inclinations of $i = e\sqrt{3}$. The orbits are phased in such a way as to keep the constellation’s shape relatively stable, and inclined to the ecliptic plane by

Table I: LISA Design Characteristics. The current baseline design parameters of the LISA observatory (these are the default settings for the online *Sensitivity Curve Generator* [23]).

Parameter	LISA Default Value
Armlength	5×10^9 m
Laser Power	1 W
Laser Wavelength	1064 nm
Telescope Diameter	0.3 m
Optical Efficiency	0.3
Acceleration Noise Budget	$\sqrt{S_a} = 3 \times 10^{-15} \text{ m}/(\text{s}^2 \sqrt{\text{Hz}})$
Total Position Noise Budget	$\sqrt{S_p} = 2 \times 10^{-11} \text{ m}/\sqrt{\text{Hz}}$

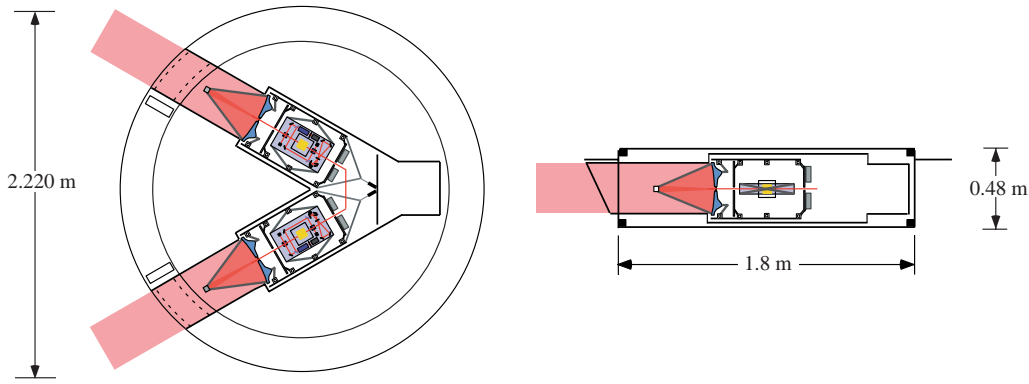


Figure 2: The basic configuration of a LISA spacecraft. Each of the three spacecraft in the constellation are replicas of each other.

60° . The shape is not perfectly stable, and the armlengths will slowly change in time. The maximum change in armlengths is only a few percent, but this will have important consequences in how interferometry is performed in the LISA system. Detailed descriptions of the spacecraft orbits, suitable for simulation purposes, have been worked out and published in the literature [24–26].

The individual spacecraft which make up the LISA observatory are shaped like hockey pucks, just over 2 meters in diameter, and about 50 centimeters high, as shown in Figure 2. The primary structure of the spacecraft is a cylinder which supports the sun-shield and solar array, as well as the articulated “Y” shaped superstructure that holds two optical systems responsible for sending and receiving laser signals with adjacent spacecraft. The articulation allows for fine pointing control of the telescope, a necessity brought on by the fact that the armlengths (and hence the shape of the constellation) are slowly changing in time.

Each optical bench sports a 30 cm Cassegraine telescope which transmits and receives the laser signals exchanged between spacecraft. At the center of the optical bench is an accelerometer system which monitors a 1 kg *proof mass* which acts as the end mirror in the interferometer arm. The proof mass is cubic in shape, and made of an alloy of about 90% gold and 10% platinum, chosen to reduce the magnetic susceptibility. The optical bench itself is manufactured as a single monolithic structure out of a large plate of ultra-low expansion material, and houses the optical network necessary to shape and monitor the laser system inputs and outputs. Laser information is exchanged with the companion optical bench on a single spacecraft through an optical fiber, allowing a single spacecraft to act in a fashion consistent with a single corner station in a traditional table-top interferometer. A simplified representation of the optical bench is shown in Figure 3, with the laser pathways shown (figure follows example in [27]).

The output laser power is only 1 W. Ideally, the laser output from the telescopes would be perfectly collimated, with the output beams being parallel and non-diverging. The beams will spread somewhat, however, an effect magnified by the fact they are propagating 5 million kilometers between spacecraft. A simple way to estimate this size is to assume a Gaussian beam profile, with the waist of the beam at the aperture of the transmitting telescope. In this case, the power P_r received at the spacecraft a distance L away, after transmitting power P_t in laser light of wavelength λ through a telescope of diameter D is[20]:

$$P_r = 0.5 \frac{D^4}{\lambda^2 L^2} P_t, \quad (1)$$

yielding a received power of $P_t = 143$ picowatts for the LISA standards listed in Table I. Approximating the initial 1 W output is uniformly spread over a circular area, the size of the beam spot is over 25 km in diameter! In reality, the power in the beam spot is not uniform; in an optimal flight configuration, the receiving spacecraft will sit as close to the center of the laser spot as possible, where the received power will be highest.

It is clear from this simple calculation that LISA cannot operate as a normal interferometer, reflecting the received light off of a local mirror and back to the spacecraft of origin! Instead, the signals are transponded; six independent signals comprise the primary laser signals in the three arms that will be used to create the main interferometric

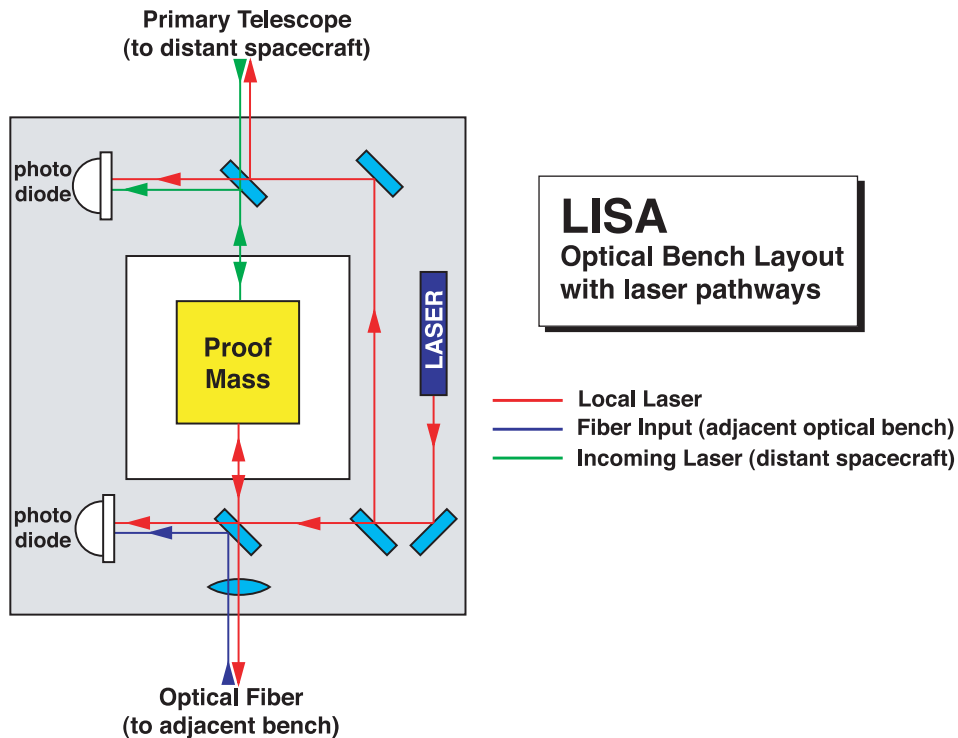


Figure 3: A simplified schematic of a LISA laser bench, showing the laser pathways and their interaction with the test mass, primary telescope (outgoing and ingoing beams) and photodiode detectors (figure follows the example of [27]).

data streams. The independent laser links may be thought of as Doppler delay lines, and the treatment of their response to an incident gravitational wave is a straightforward adaptation of the analysis used to describe Doppler tracking of spacecraft for gravitational wave detection [6–8]. To allow LISA to function as an interferometer in this arrangement, a sophisticated scheme for phase locking six independent lasers on the three spacecraft is being devised. Faint incoming laser signals are monitored, and refreshed full power beams are retransmitted back down the arm. As a consequence, no direct generation of a primary interferometric data stream is physically generated on orbit. The phases of the exchanged laser signals are monitored and stored, and later recombined (in software) to create the primary interferometric signals using a technique called *time delay interferometry* (TDI, described in more detail in § 2.2).

2.2. Time Delay Interferometry

Unlike ground-based interferometric observatories, LISA will not be a static instrument. Each individual spacecraft is on its own independent Keplerian orbit, and constantly in motion relative the other spacecraft in the constellation. As a result, the armlengths are continuously changing in time; the arms “breathe” in an oscillatory way as a function of time, as shown in Figure 4.

In a classic Michelson interferometer¹, the two arms are equal in length. Noise associated with fluctuations in the laser automatically cancels out in a Michelson interferometer because the fluctuations propagate down the two arms and return back to the beam splitter at the same time, where the interference of the two signals cancels out the fluctuations.

¹In simple treatments of laser interferometer observatories, the fundamental interferometric observable is often approximated to be equivalent to that of a classic Michelson interferometer.

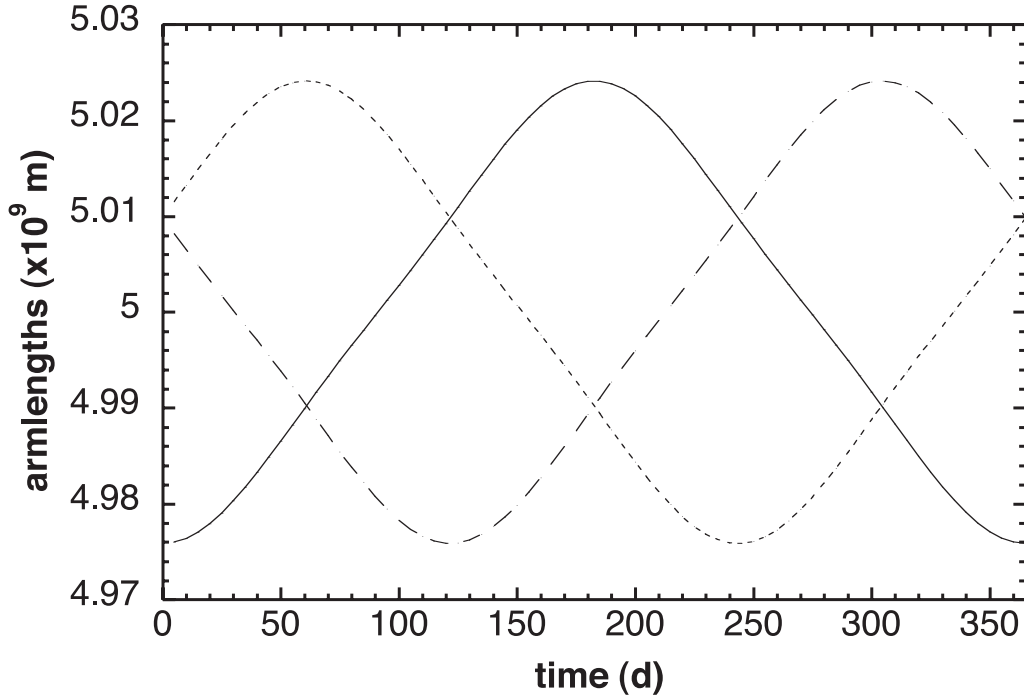


Figure 4: The three LISA armlengths will “breathe” over the course of a full LISA orbit (1 year). This simulation of the time-variation of the armlengths was computed from the LISA spacecraft orbits described in [26].

In an instrument like LISA, the armlengths are continuously changing in time. Envisioning the observatory like a classic Michelson interferometer, where one spacecraft plays the role of a corner station (vertex) where the laser is divided and recombined, and the two adjacent spacecraft play the roles of stationary mirrors at the end stations of the interferometer, one can easily see how the changing armlengths can be a problem. Suppose the primary laser signal develops a random fluctuation in its frequency output. That fluctuation is propagated down each of the two arms, is transponded (equivalent to reflection) off the distant spacecraft at the ends of the arms, and returns back to the original vertex of the interferometer. If the arms are unequal in length and changing in time, the fluctuations will arrive back at the vertex at different times and do not cancel out. This is a serious problem because the expected noise associated with fluctuations in the LISA laser system is several orders of magnitude larger than any other source of instrumental noise in the system. Fortunately, there is way to mitigate these issues, called *time delay interferometry* (TDI).

Consider the constellation schematic shown in Figure 5, where each of the three spacecraft is identified by a numeral $\{1, 2, 3\}$, and the arm opposite a given spacecraft bears the same numeric name $\{L_1, L_2, L_3\}$. The guiding center is the geometric point which is equidistant from each of the three spacecraft. The guiding center distance is given in terms of the three armlengths by

$$\ell = \frac{L_1 L_2 L_3}{\sqrt{2L_1^2 L_2^2 + 2L_2^2 L_3^2 + 2L_1^2 L_3^2 - L_1^4 - L_2^4 - L_3^4}}. \quad (2)$$

In traditional Michelson interferometry, the interferometric data is constructed as the phase difference between the laser signals in two arms of the interferometer, each measured at the same time t . If the phase a spacecraft measures from the signal arriving along arm L_i is denoted $s_i(t)$, then the traditional Michelson signal which would be measured at spacecraft 3, $\Delta_3(t)$, would be written as:

$$\Delta_3(t) = s_1(t) - s_2(t). \quad (3)$$

In time delay interferometry, the six independent laser phase signals are taken in linear combinations, and at times which are shifted with respect to the absolute time t which indexes the data stream. Consider the unequal-arm

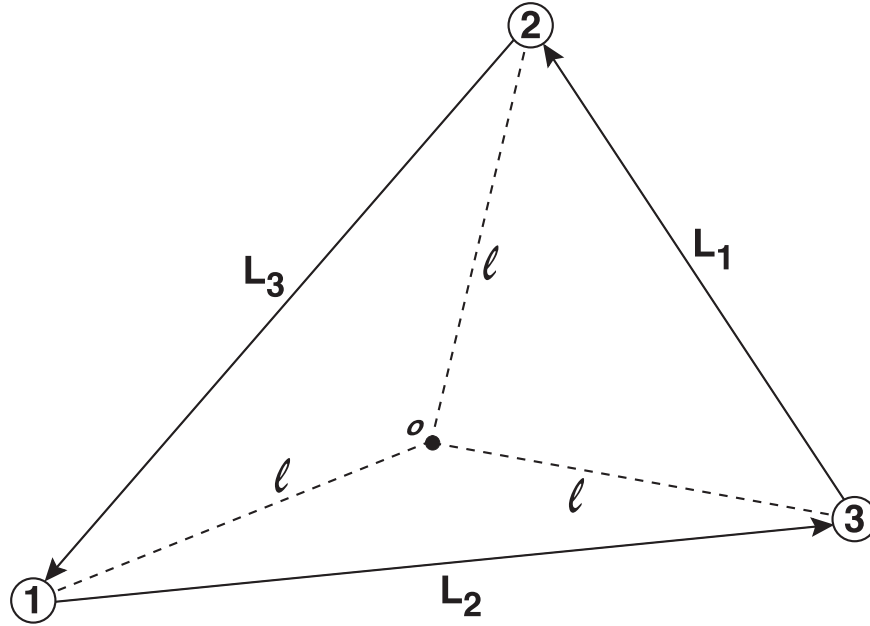


Figure 5: A simple naming scheme for construction of TDI observables. Each spacecraft is identified by an arabic numeral, $\{1, 2, 3\}$, and the opposing armlength is identified by the same numeral, $\{L_1, L_2, L_3\}$, as indicated. Because the armlengths are changing in time and the shape is slowly varying, it is often useful to identify the geometric point o , which is equidistant from each of the three spacecraft. The distance ℓ is usually called the *guiding center distance*. The inequality of the armlengths and the distortion of the constellation shape has been greatly exaggerated for clarity.

Michelson TDI combination, which is conventionally given the name $X(t)$ at a single vertex. If the one way light travel time down arm i is denoted $\tau_i = L_i/c$, then the unequal arm Michelson TDI variable is written in a simple guise as²

$$X(t) = s_1(t) - s_1(t - 2\tau_2) - s_2(t) + s_2(t - 2\tau_1) , \quad (4)$$

which looks like the standard equal-arm Michelson signal with additional *time-delayed* bits subtracted off. As an interferometric technique, TDI takes the measured phase information from each arm, and delays the linear combinations in such a way as to make the optical path lengths in the two phase signals equal³ [29–31], thereby creating a situation where particular types of noise cancel out when the beams are differenced.

TDI data streams come in related triples – for any given possible combination (like the example written in Eq. 4), there are two related variables which are obtained by exploiting a well known “permutation symmetry” whereby the identifying indices are permuted $1 \rightarrow 2 \rightarrow 3 \rightarrow 1$. The two companion data streams to $X(t)$ are called $Y(t)$ and $Z(t)$. Utilizing the permutation symmetry, and starting from Eq. 4 they may be written as

$$Y(t) = s_2(t) - s_2(t - 2\tau_3) - s_3(t) + s_3(t - 2\tau_2) \quad (5)$$

and

$$Z(t) = s_3(t) - s_3(t - 2\tau_1) - s_1(t) + s_1(t - 2\tau_3) \quad (6)$$

Other important TDI triples which appear in the literature are $\{\alpha, \beta, \gamma\}$ (the so-called *Sagnac combinations* [28]), and $\{A, E, T\}$ (the so-called *optimal combinations*[32]).

²For a full expression of $X(t)$ with geometric factors and time delays written out in full glory, see [28].

³In essence, the TDI combinations synthesize equal-arm interferometric signals, as shown geometrically in [29].

TDI has evolved since its inception, and is now arranged into different generations, corresponding to the inclusion of higher order motion effects in the time delay corrections [30, 31, 33, 34]. General results derived from first generation TDI [27, 28] are expected to carry forward and still hold true in later generations as the corrections are small and “easy” (in some sense) to account for; general results derived for first generation TDI variables should have corresponding valid counterparts in higher generations. As modern tools for generating LISA data streams are becoming available (*e.g.*, *Synthetic LISA* [35] and *The LISA Simulator* [36]), they are automatically building these higher order TDI signals into their architecture.

Figure 6 shows the possible interferometric topologies which LISA could employ [27]; each has a moniker which accurately describes the behaviour of the instrument when operating in that mode. As with every TDI variable, each of these modes has a slightly different sensitivity, and will yield different instantaneous sky sensitivity. Perhaps more importantly, these modes illustrate the ways in which LISA can function should an instrumental failure occur while the observatory is on orbit. Careful inspection of each of these modes will show that LISA can survive the loss of any two of the six laser links between spacecraft; the loss of an entire spacecraft would be catastrophic (removing four laser links), and effectively cripple the mission⁴.

An extensive review of the fundamentals of TDI may be found in [38].

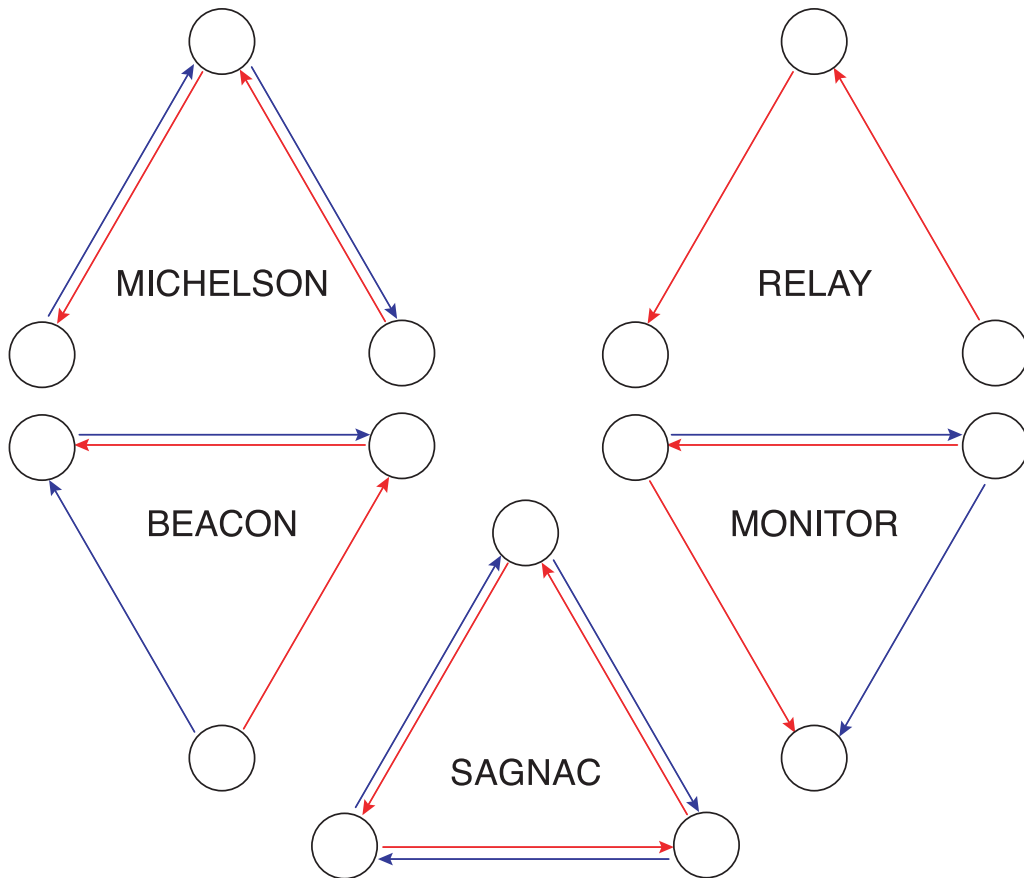


Figure 6: Five basic laser topologies are possible using TDI and the six laser signals exchanged between the three spacecraft, known as *Michelson*, *relay*, *beacon*, *monitor* and *Sagnac* (after [27]).

⁴Even with the loss of an entire spacecraft, it may still be possible to operate the two remaining spacecraft as a *xylophone detector* [37].

2.3. TDI Applications

TDI, aside from being necessary to make long-baseline laser interferometry in space possible, has many interesting applications which make it an invaluable tool for gravitational wave astronomy.

One of the first things a careful student of TDI will notice, is that the sensitivity curves for different TDI variables have different shapes across the LISA frequency band. Overall, the sensitivities are all very similar, but it raises the intriguing possibility that if a compelling astrophysical argument could be made to reshape the sensitivity curve to provide observational access to a particularly interesting source, the choice of appropriate TDI variables can provide some flexibility.

A particular Sagnac combination, usually denoted $\zeta(t)$, has the interesting property that it is insensitive to gravitational waves at low frequencies. At frequencies below the transfer frequency, $f_* \sim c/(2\pi L_o) \simeq 10$ mHz, the response to gravitational waves is suppressed by roughly a factor of 1000 [27, 28]. By contrast, instrumental noise is *not* suppressed. It has been suggested [39] that this provides a method whereby the LISA instrumental noise can be validated while the observatory is on-orbit. A deconvolution of the $\zeta(t)$ data channel should yield, at low frequencies, the pure instrumental noise uncontaminated by any but the strongest astrophysical signals. In a similar vein, it has been suggested [40] that a similar procedure can be used to determine how much of the observed low frequency signal coming out in a data stream is instrumental noise, and how much is simply confused astrophysical noise (*e.g.*, from the galactic population of compact binaries, or a stochastic cosmic gravitational wave background).

Another important TDI application related to the $\zeta(t)$ signal is the *zero signal solution* (ZSS) [41, 42]. The ZSS can be used to determine the sky location of gravitational wave sources without exploiting the modulation produced by LISA's yearly motion around the Sun. The technique takes linear combinations of a TDI triad which reduce to a function characterized by two parameters, namely the sky location angles $\{\theta, \phi\}$. When a gravitational wave signal is present in the data, it can be “zeroed out” by searching for the values of $\{\theta, \phi\}$ which minimize the ZSS. In essence, the technique uses the time of flight of a gravitational wave signal across the LISA constellation to construct a triangulation of the source location. At high frequencies, a signal can be precisely zeroed out (to the level of the instrumental noise). At low frequencies, gravitational wave signals cannot be zeroed out; they can only be suppressed in a fashion similar to $\zeta(t)$. This low frequency behaviour can be understood using the time-of-flight view of how the ZSS works; at low frequencies, the gravitational wavelength is larger than the entire LISA constellation, and so it is impossible to determine the direction a gravitational wave is coming from because the observatory is contained inside a single cycle of the wave which is slowly varying on timescales long compared to the time of flight down the interferometer arms. Because it does not employ Doppler modulation generated by LISA's motion around the Sun, the ZSS is particularly useful for burst localization on the sky. A simple estimate of the pointing accuracy of the ZSS is⁵:

$$\Delta\Omega = \frac{2c^2}{\pi^2 A \cos(\alpha) f_o^2 \rho^2} \quad (7)$$

where f_o is the frequency of the gravitational wave, c is the speed of light, A is the area enclosed by LISA constellation, ρ is the SNR of the observed signal, and α is the angle between the gravitational wave propagation vector and the normal to the LISA plane.

3. LISA AS AN OBSERVATORY

Once the rockets have done their job, the spacecraft are in their respective orbits, and the first laser links have been acquired, LISA will transition from being a mission to being a viable astrophysical observatory. In a very real sense,

⁵This form of the solid angle error $\Delta\Omega$ is an adaptation of Eq. (8.5) in [43], a closely related technique for arrays of ground-based interferometric observatories.

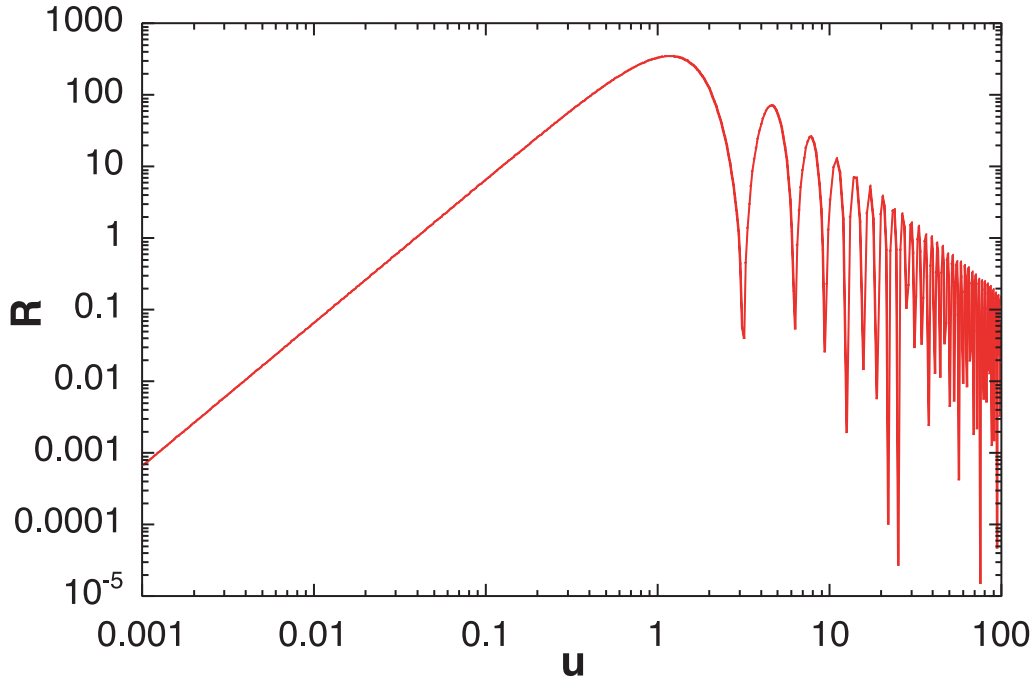


Figure 7: The $X(t)$ gravitational wave transfer function, $\mathcal{R}(u)$, for near equal armlengths, plotted versus the dimensionless quantity $u = 2\pi f\tau$, where τ is the time of flight down one arm of the interferometer. This transfer function has been averaged over all sky positions and all polarization states. This treatment of the transfer function follows [45].

LISA's ability to observe the Universe as part of an observational enterprise depends crucially on understanding the strength of prospective sources and the instruments ability to resolve those sources. This section looks at how the LISA sensitivity is constructed (§ 3.1), simple ways to estimate source strengths (§ 3.2), and how the combination of the two can be combined to make predictions about the science capability of the observatory (§ 3.3).

3.1. LISA Sensitivity

Estimating the expected LISA sensitivity as a function of gravitational wave frequency has been an active industry for some time [27, 28, 44–47]. The matter is also confused by several common approximations [48, 49], which are often extended and used in regimes where they are not valid. Recent work has looked at various low frequency approximations and provided some guidance for the ranges of validity [26, 50]. Much of the confusion surrounding the use of general sensitivity curves has been mitigated by the LISA project's advocacy of a standard tool [23] which has been tested and shown to be consistent with standard versions of the sensitivity which have propagated through the literature and are in use by the project.

The basic theory of the LISA sensitivity can easily be understood in simple terms by schematically identifying how it is constructed. The principle players in the description of a sensitivity curve are the power spectral density of the instrumental noise, $S_n(f)$, the noise transfer functions, $\mathcal{R}_n(f)$, and the gravitational wave transfer function $\mathcal{R}(f)$. In principle, the instrumental noise is a composite of several different noise processes, $\{S_1, S_2, \dots\}$, each of which has its own noise transfer function, $\{\mathcal{R}_1, \mathcal{R}_2, \dots\}$.

Transfer functions⁶ describe the response of an instrument, as a function of frequency, to signals which are incident upon it; in essence, a mapping between input and output frequencies of the observatory. The form of the transfer

⁶Also sometimes referred to as *response functions*.

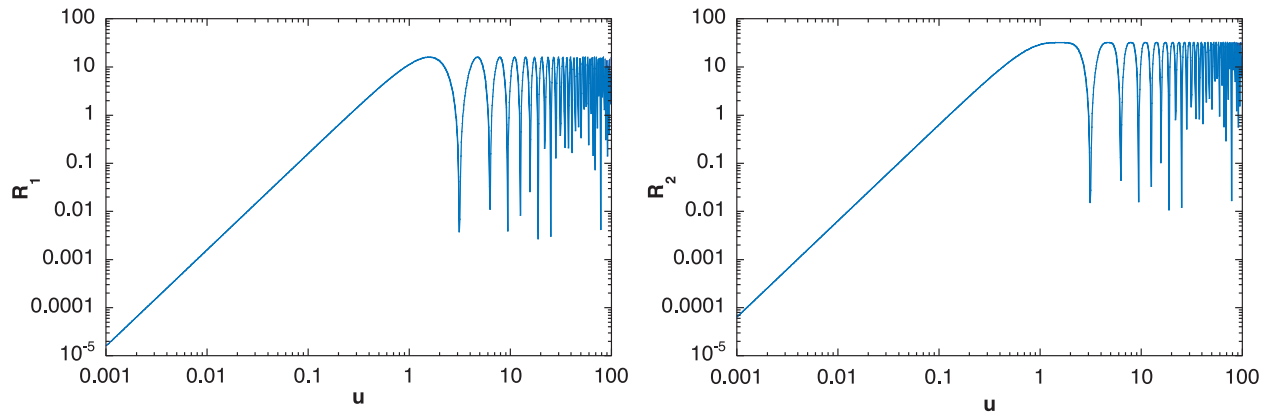


Figure 8: $X(t)$ noise transfer functions for near equal armlengths, plotted versus the dimensionless quantity $u = 2\pi f\tau$. The left pane shows the transfer function for position noise, $\mathcal{R}_1(u)$, and the right pane shows the transfer function for acceleration noise, $\mathcal{R}_2(u)$. This treatment of the transfer functions follows [45].

function depends on the choice of interferometric variable being used, and must be derived for both gravitational waves and different sources of noise. Figure 7 shows the gravitational wave transfer function, averaged over all sky positions and all polarization states, plotted versus the dimensionless quantity $u = 2\pi f\tau$, where τ is the time of flight down one arm of the interferometer. Figure 8 shows the transfer functions for acceleration and position noises when the $X(t)$ TDI variable is used.

Noise for observatories like LISA is generally classified into two broad categories: *acceleration noise* and *position noise*. Each category has many different constituents contributing to it at various levels. For example, acceleration noise is comprised of sources such as thermal distortion of the spacecraft, electrical forces on the test masses, residual gas impacts, and many others. Similarly, position noise is a composite of sources such as laser shot noise (the single largest source), residual laser phase noise, and pointing instabilities. Extensive lists of the “noise budgets” for position noise and acceleration noise may be found in Tables 4.1 and 4.2, respectively, of the LPPA [20]. These budgets characterize the allowable contributions from each source of noise if the overall performance requirements for the observatory are to be met. Figure 9 shows the expected rms composite noise spectrum for the LISA observatory operating at the mission specifications⁷. The figure clearly shows the two regimes. At low frequencies, the spectrum is dominated by steeply rising acceleration noise⁸, whereas at high frequencies the spectrum is dominated by the flat profile of the position noise.

As illustrated here, this is a purely idealized representation of the noise, though numerical simulations designed to model the injection of instrumental noise into the LISA signals show similar character[26]. The true noise spectrum will almost certainly have fluctuations and structure, and have slope and character which deviate from the simple power law predictions shown here. One important aspect of the LISA noise which is sometimes hinted at in the literature, but which has yet to be specified, is the very low frequency performance of the observatory. Somewhere between $f \sim 10^{-4}$ Hz and $f \sim 10^{-5}$ Hz, the acceleration performance is expected to become much worse, effectively forming a low-frequency cutoff for the observatory. Exactly characterizing this cutoff, and engineering around it is difficult owing to the long timescales involved with processes which shape the spectrum at low frequencies. Where the cutoff falls can have important implications for LISA’s capabilities as an astrophysical observatory (see, *e.g.*, [51, 52]).

The noise spectra and transfer functions are combined to estimate the sensitivity of the observatory as a function

⁷The treatment shown in the figure follows [45] which predicts the functional form of the noise. Numerical simulations of the expected instrumental noise spectrum have also been produced in the literature, notably in [26].

⁸Sometimes this is called *red noise* because it is stronger at lower frequencies.

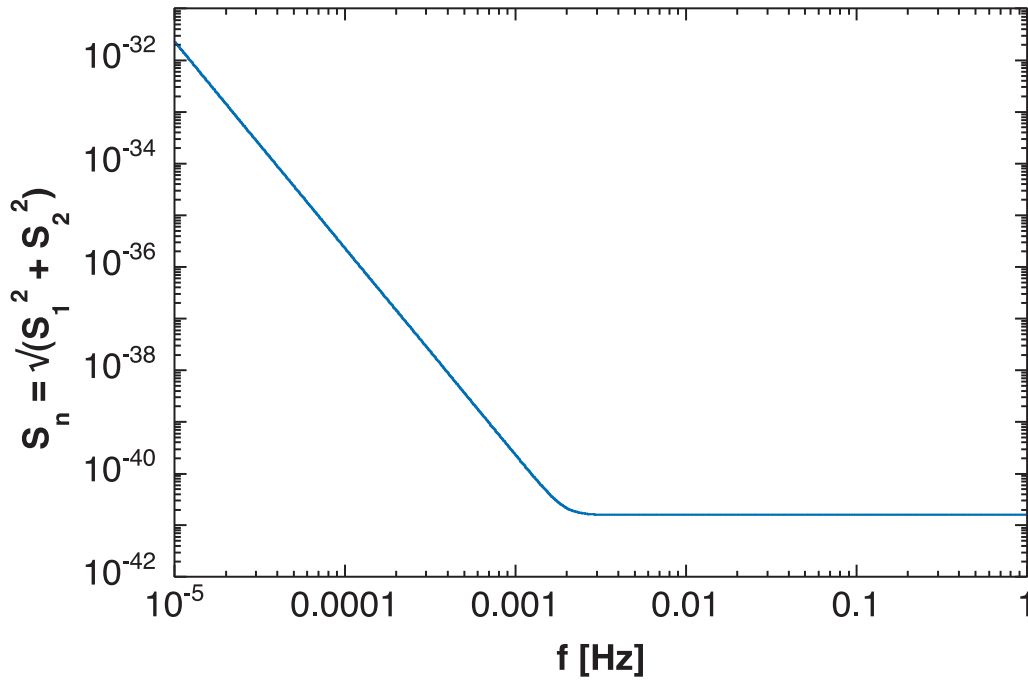


Figure 9: Expected LISA rms noise spectrum, as a function of observed frequency. The sharp rise at low frequencies is set by the acceleration performance of the instrument, whereas the floor is set by the position noise performance of the instrument. This treatment of the noise follows [45].

of gravitational wave frequency f . It is conventional to plot the *spectral amplitude* $h_f^L(f)$ which is related to the noise spectra and transfer functions as⁹

$$h_f^L(f) = \sqrt{\frac{S_n \cdot \mathcal{R}_n}{\mathcal{R}}}, \quad (8)$$

and has units of $1/\sqrt{\text{Hz}}$. The general representation of the sensitivity is more appropriately written as

$$h_f^L(f) = \sqrt{\frac{S_1 \cdot \mathcal{R}_1 + S_2 \cdot \mathcal{R}_2 + \dots}{\mathcal{R}}}. \quad (9)$$

The standard LISA sensitivity curve is shown in Figure 10. Note that the curve extends down to $f = 10^{-5}$ Hz, into the regime where the low-frequency performance is not well understood or characterized.

Much comparison is often made between ground-based detectors like LIGO and spaceborne detectors like LISA; indeed, much of the mathematical machinery used to describe gravitational wave detection for ground based observatories has carried over to the LISA literature. With this in mind, it is useful to note that in the context of LIGO one often talks about “noise curves” because the gravitational wave transfer functions are roughly constant at the frequencies covered by the detectors, doing nothing to the *shape* of the detector noise as a function of frequency, only scaling it by a constant. By contrast, the LISA gravitational wave transfer function *is* a function of frequency, significantly modifying the shape of the noise, particularly in the regime where the detector arms are long compared to a gravitational wavelength. The practical use of the phrase “noise curve” in the literature is to represent the threshold strength a source needs to have to be seen above all other effects related to the instrumental performance. This is still the case with a sensitivity curve; the instrumental response function alters the required strength a signal

⁹The superscript L denotes the value of the spectral amplitude for the LISA detector, as opposed to the spectral amplitude for a source, discussed in later sections.

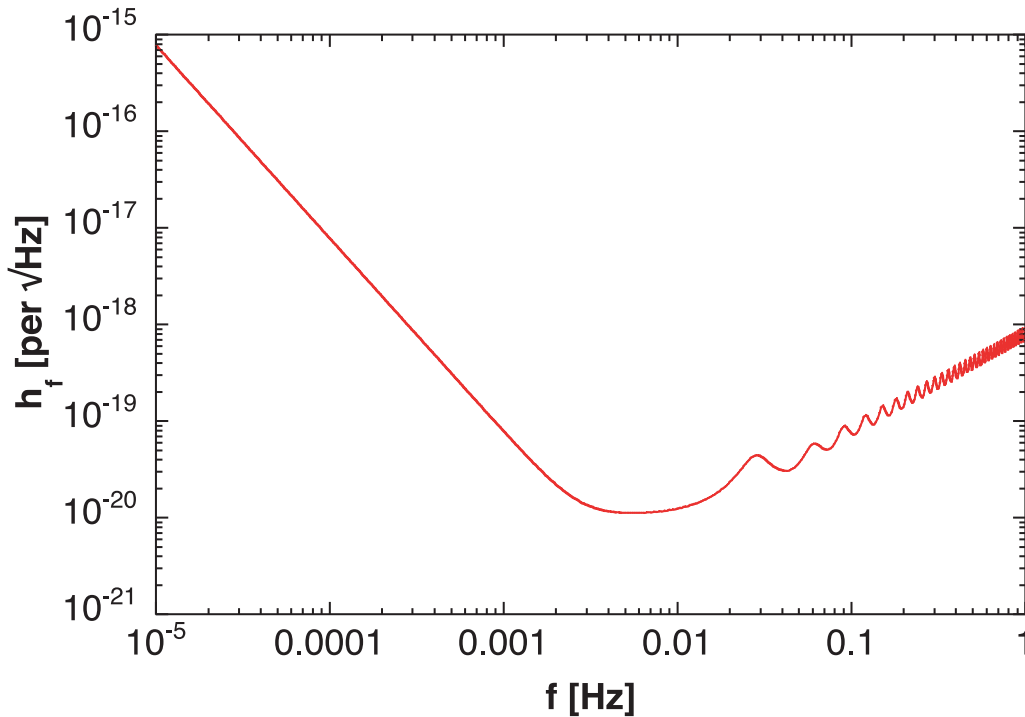


Figure 10: The standard LISA sensitivity curve, where the instrumental threshold corresponds to sources with $SNR = 1$. The region above the threshold curve is generally referred to as the *LISA discovery space*. This sensitivity curve was generated by the *Online Sensitivity Curve Generator* [23] at its default settings.

needs to have to be detectable. In the strictest sense, however, the term *noise curve* most appropriately refers to a quantity like that plotted in Figure 9. In the LISA context, a *sensitivity curve*, shown in Figure 10, describes the instrument’s capabilities as an astrophysical observatory, and folds in aspects of the instrumental noise with the instrument response function.

As a general rule, the average end user interested only in the LISA sensitivity from the standpoint of evaluating prospects for potential observations of an astrophysical source does not need to worry about the nuances of transfer functions and the mechanics of constructing a sensitivity curve. It *is* important, however, to be aware that the sensitivity is not plotted the same by everyone in the literature, and that some representations are more suited than others for particular astrophysical applications. The two most common representations of the sensitivity are plots of the *dimensionless strain* h^L , and plots of the *spectral amplitude* (or *root spectral density*) h_f^L . Making a choice of sensitivity curve to use in a given computation is discussed at greater length in section 3.3.

Another common habit that appears repeatedly in the LISA literature is to plot sensitivity curves “for signal-to-noise ratio of 5”¹⁰. The basic assumption in this approach is that the pictorial representation of the instrumental sensitivity should account for the fact that gravitational wave data analysis is difficult and sources will likely not be detectable if their strength is only equal to that of the instrumental threshold; to make up for that belief, the sensitivity curves are shifted *up* by a factor of 5. It has become more common in the recent literature to simply plot sensitivity curves for SNRs of 1, with the understanding that sources only marginally above the sensitivity are likely inaccessible. In general, the threshold sensitivity curve can be written as

$$h_f^L(f) = \rho_o \sqrt{\frac{S_n \cdot \mathcal{R}_n}{\mathcal{R}}}, \quad (10)$$

¹⁰This is the habit, for instance, in the LPPA [20].

where ρ_o is the desired threshold SNR at the level of the curve. For all the figures in this article, $\rho_o = 1$. Readers of the LISA literature are advised to beware of these issues, and carefully consider any plot they encounter.

3.2. Gravitational-wave sources

Binary systems are the subject of much attention in gravitational wave astronomy because in the bands accessible to modern broadband interferometric detectors, they are expected to be among the most prevalent of sources. To that end, it is useful to have in hand pocket formulae which are convenient for quickly estimating source characteristics.

For circularized binaries which are evolving slowly, the gravitational wave emission is characterized by

$$\text{chirp mass} \quad \mathcal{M}_c = \frac{(m_1 m_2)^{3/5}}{(m_1 + m_2)^{1/5}} \quad (11)$$

$$\text{scaling amplitude} \quad h_o = \frac{\mathcal{M}_c}{D} (\pi f \mathcal{M}_c)^{2/3} \quad \Rightarrow \quad \frac{G}{c^2} \frac{\mathcal{M}_c}{D} \left(\frac{G}{c^3} \pi f \mathcal{M}_c \right)^{2/3} \quad (12)$$

$$\text{chirp} \quad \dot{f} = \frac{96}{5} \frac{f}{\mathcal{M}_c} (\pi f \mathcal{M}_c)^{8/3} \quad \Rightarrow \quad \frac{96}{5} \frac{c}{G} \frac{f}{\mathcal{M}_c} \left(\frac{G}{c^3} \pi f \mathcal{M}_c \right)^{8/3} \quad (13)$$

where the equations on the right side of the \Rightarrow have had conventional units restored to facilitate simple applications in astrophysical scenarios¹¹. The phase $\phi(t)$ of the binary evolves in time as

$$\phi(t) = 2\pi \left(f t + \frac{1}{2} \dot{f} t^2 \right) + \phi_o, \quad (14)$$

where \dot{f} is the chirp given by Eq. 13, and ϕ_o is the initial orbital phase of the binary. This simple linear description of a binary chirp can be used to estimate the time it takes a circularized binary to evolve between any two frequencies f_1 and f_2 by integrating the first order differential equation in Eq. 13 to yield

$$\Delta t = \kappa \left[f_1^{-8/3} - f_2^{-8/3} \right] \quad (15)$$

where

$$\kappa = \frac{5}{256} \mathcal{M}_c^{-5/3} \pi^{-8/3} \quad \Rightarrow \quad \frac{5}{256} \left(\frac{G}{c^3} \mathcal{M}_c \right)^{-5/3} \pi^{-8/3}. \quad (16)$$

This type of analysis is common in gravitational wave physics, and is the foundation for the classic treatment of binary evolution by Peters and Mathews [53, 54], which treat not only circularized binaries, but also eccentric binaries.

The time to coalescence, t_c , is a favored parameter in gravitational wave astrophysics because it embodies a binary system's current evolutionary state, and because it embodies when a gravitational wave signal will end for observations of the late stages of inspiral. For a binary which is observed at a frequency f_1 , a simple estimate of t_c can be obtained from Eq. 15 by setting f_2 equal to the penultimate frequency the binary will have before merger. In many instances, the binary components are treated simply as point masses, and the inspiral ends when their separation goes to zero and $f_2 \rightarrow \infty$. This is the case in the classic treatments of Peters and Mathews [53, 54], who express the lifetime, τ_{gw} , as an integral over the eccentricity

$$\tau_{gw} = \tau_o \int_0^{e_o} de \frac{e^{29/19} [1 + (121/304)e^2]^{1181/2299}}{(1 - e^2)^{3/2}}, \quad (17)$$

¹¹If one wishes to use the equations written in geometricized units, on the *left* side of the \Rightarrow , then a useful conversion factor to know is: $1M_\odot = 1476.687\text{m} = 4.925698 \times 10^{-6}\text{s}$.

where the scaling constant τ_o is expressed in terms of the initial pericenter r_{p_o} and initial eccentricity e_o of the orbit:

$$\tau_o = \frac{15}{304} \frac{r_{p_o}^4 (1 + e_o)^4}{m_1 m_2 (m_1 + m_2) e_o^{48/19}} \left[1 + \frac{121}{304} e_o^2 \right]^{-3480/2299}. \quad (18)$$

The Peters and Mathews inspiral lifetime for a circular orbit with initial radius a_o is given by

$$\tau_{circ} = \frac{5}{256} \frac{a_o^4}{m_1 m_2 (m_1 + m_2)}. \quad (19)$$

Note that this expression for τ_{circ} can be derived from Eq. 15 by letting $f_2 \rightarrow \infty$ (equivalent to letting the orbital period go to zero)¹².

For binary systems which involve black holes, the inspiral stage is taken to end when the frequency evolves to the frequency of the innermost stable circular orbit (ISCO)¹³. Conventional descriptions for the ISCO come out of pure gravitational theory, and again are generally only valid for point particles; it is not clear if the ISCO is well defined in the equal mass limit, or even if there is such a thing as an ISCO for extended bodies. To circumvent this problem, a helpful approach is to make a conservative estimate of the frequency at which an inspiraling body makes the transition from inspiral to plunge. One useful approximation, motivated by a variety of studies looking for the ISCO, takes the coalescence frequency to be [51]

$$f_c = 41 \text{mHz} \left(\frac{10^5 M_\odot}{m_1 + m_2} \right). \quad (20)$$

Chirping binaries are of particular interest in gravitational wave astrophysics, as they enable a way to accurately determine the distance to the gravitational wave source, independent of any other observations. This can be seen by considering the chirp in Eq. 13 and the binary amplitude in Eq. 12. If the chirp \dot{f} at a given frequency f can be measured, then Eq. 13 can be solved for the chirp mass:

$$\mathcal{M}_c = \left[\frac{5}{96} \pi^{-8/3} f^{-11/3} \dot{f} \right]^{3/5}. \quad (21)$$

With the chirp mass, and the measured amplitude h_o at frequency f , then Eq. 12 can be solved for the distance to the binary:

$$D = \frac{\mathcal{M}_c}{h_o} (\pi f \mathcal{M}_c)^{2/3} = \frac{5}{96 \pi^2} \frac{1}{h_o} \frac{\dot{f}}{f^3}. \quad (22)$$

More detailed descriptions of gravitational wave generation for generic binary motion, particularly in cases where Keplerian orbits are adequate for describing the trajectories of binary components are discussed at great length in the literature [53, 54, 56]. For many binaries in the LISA band, these treatments should be adequate, valid at quadrupolar order. For highly relativistic, strong field binaries, higher order Post-Newtonian waveforms (see *e.g.*, [57]¹⁴) may be necessary to make adequate estimates of the gravitational wave emission.

When discussing the strength of gravitational waves, it is often useful to be able to construct conventional astrophysical quantities from the dimensionless strain h , which for binaries scales with the amplitude in Eq. 12. Particularly useful quantities in astrophysics are the *luminosity*, \mathcal{L} , which characterizes the amount of energy per unit time the gravitational waves are carrying away from the system, and the *flux*, \mathcal{F} , which characterizes the power per unit area

¹²To accomplish this derivation, you will need to make judicious use of Kepler's third law, and the fact that for circular orbits, the gravitational wave frequency is related to the orbital frequency by $f = 2f_{orb}$.

¹³For binaries where the primary is a black hole of mass M_\bullet and the orbit has an eccentricity e , an equivalent condition is that inspiral ends (the binary plunges) when the pericenter of the orbit is less than the radius of the *unstable circular orbit* located at [55]: $r_{uco} = 2M_\bullet(3 + e)/(1 + e)$.

¹⁴Another treatment of the waveform calculations outlined in [57], useful for LISA applications, is derived in [58].

is received at a given distance from a source. Writing generic expressions for these quantities is difficult due to the variety of sources which are of potential interest in the LISA band¹⁵. If one restricts attention to binaries, then simple expressions have been worked out for the average luminosity[53]

$$\mathcal{L} = \frac{32}{5} \frac{(2\pi f_{orb} \mathcal{M}_c)^{10/3}}{(1-e^2)^{7/2}} \left(1 + \frac{73}{24} e^2 + \frac{37}{96} e^4 \right), \quad (23)$$

where $f_{orb} = 1/P_{orb}$ is the orbital frequency of the binary. When considering only a small part of the emitted gravitational waves (*e.g.*, the part of the wavefront subtended by a detector), it is often more useful to think in terms of the gravitational wave flux \mathcal{F} . For the averaged luminosity in Eq. 23, the flux is defined from the luminosity as

$$\mathcal{F} = \frac{\mathcal{L}}{4\pi D^2} = \frac{8}{5\pi D^2} \frac{(2\pi f_{orb} \mathcal{M}_c)^{10/3}}{(1-e^2)^{7/2}} \left(1 + \frac{73}{24} e^2 + \frac{37}{96} e^4 \right), \quad (24)$$

when the binary is a distance D away. For circular ($e = 0$) binaries¹⁶, comparison with Eq. 12 shows that the flux scales as¹⁷ $\mathcal{F} \propto (fh_o)^2$, and the luminosity scales as $\mathcal{L} \propto (fh_o D)^2$.

3.3. How strong is a source?

Gravitational wave astronomy is rich in terms of the variety and number of different sources which will be accessible to the current generation of observatories. At the same time, the field is in its infancy as an observational science, and as observers we are still learning the ropes in our efforts to best describe and explain our science to our colleagues and the rest of the astronomical community. These two facts have given rise to a plethora of ways to represent the strength of gravitational wave signals and their relationship to the sensitivity of our detectors. Several common representations are repeatedly encountered in the literature.

Far and away the most intuitive quantity to think about and plot is simply *dimensionless strain* h , as this is the quantity which most closely ties to the theoretical foundations of general relativity which gave rise to gravitational wave astronomy. As an observational quantity, h depends on the time evolution of the mass distribution in the source. It was Einstein himself who first derived the now famous *quadrupole formula* [60] which expresses the strain in terms of time derivatives of the reduced quadrupole moment tensor $I_{ab}(t)$ of the mass distribution:

$$h_{ab} = \frac{2}{r} \ddot{I}_{ab}(t-r). \quad (25)$$

Evaluating the quadrupole formula for a binary in a Keplerian orbit will reveal the scaling noted in Eq. 12.

When attempting to plot the relationship between the strength of a source and the instrumental sensitivity, it is important to choose an appropriate representation, and to plot the *same* quantity for the source and sensitivity curve.

A favored quantity to plot is the *spectral amplitude*, $h_f(f)$, which is the same quantity the sensitivity is described in terms of in Eq. 8. Different types of sources require different methods of constructing a spectral amplitude suitable for plotting on such a sensitivity curve.

Continuous sources, such as stationary, circular (monochromatic) galactic binaries narrow their bandwidth Δf when observed for long periods of time T_{obs} . If the binary has strain amplitude h_o at frequency f , then it will look

¹⁵In general, if one knows either the time dependent quadrupole moment of the system, or the time dependent waveform amplitudes (derived from the quadrupole moment), then one can compute the anisotropic flux and luminosity from any astrophysical system of interest. Extensive discussion of computing radiated energy and angular momentum in astrophysical systems may be found in Chapter 36 of [59].

¹⁶For circular binaries, the gravitational wave frequency is related to the orbital frequency by $f = 2f_{orb}$.

¹⁷This scaling is dimensionally correct and is adequate for simple computations; a proper calculation will show that the flux scales as $\mathcal{F} \propto \dot{h}^2$.

like a single spectral line in the Fourier spectrum with spectral amplitude

$$h_f(f) = \frac{h_o}{\sqrt{\Delta f}} = h_o \sqrt{T_{obs}} . \quad (26)$$

If one desires to plot the binary strain h_o rather than the spectral amplitude, the appropriate sensitivity curve is a strain curve, computed from Eq. 8 as a function of the observing time T_{obs} as

$$h^L = \frac{h_f^L}{\sqrt{T_{obs}}} . \quad (27)$$

Note that in terms of strain, the LISA sensitivity improves with extended observation time T_{obs} . For chirping binaries¹⁸, the *detectable strain* h_D at a given frequency can be plotted against the detector strain curve given by Eq. 27 by taking the scaling amplitude and multiplying by the total number of cycles N_{cy} of radiation the binary emits at a given frequency f :

$$h_D = h_o \cdot \sqrt{N_{cy}} . \quad (28)$$

If the frequency resolution of the detector is $\Delta f = 1/T_{obs}$, then the time a binary spends between two frequencies f_1 and $f_2 = f_1 + \Delta f$ (the “time in a frequency bin”) is given by Eq. 15 as

$$t_{bin} = \frac{8}{3} \kappa \frac{f_1^{-11/3}}{T_{obs}} , \quad (29)$$

where the assumption $\Delta f \ll f_1$ has been employed. At any given frequency in the LISA band, N_{cy} depends on how long a binary spends in the frequency bin around that frequency, and is given by

$$N_{cy} = f \cdot t_{bin} \simeq \frac{8}{3} \frac{\kappa}{T_{obs}} f^{-8/3} . \quad (30)$$

For bursting sources, which have short time profiles of width τ_b and maximum burst amplitude h_b , the central frequency of the burst is around $f \sim 1/\tau_b$ and the strength of the burst can be plotted on the spectral amplitude graph as

$$h_f = h_b \sqrt{\tau_b} . \quad (31)$$

Stochastic backgrounds are most often characterized in terms the strain spectral density of the background, $S_h(f)$, and is related to the energy density by

$$\Omega_{gw}(f) = \frac{4\pi^2}{3H_o^2} f^3 S_h(f) . \quad (32)$$

The threshold sensitivity of the detector to stochastic profiles $\Omega_{gw}(f)$ is plotted by evaluating Eq. 32 with $S_h(f) = (h_f^L)^2$, where h_f^L is the threshold spectral amplitude of the LISA detector defined in Eq. 8.

The strength of a stochastic backgrounds generally can't be expressed in terms of a definitive scaling amplitude h precisely because they are stochastic; they fluctuate and vary with time, so the power spectral density $S_h(f)$ is the desirable quantity to work with because it encodes the strength of the background in such a way as to describe how much variation there is in the background at a given frequency. This is a fundamental quantity associated with the background. However, it is often desirable to work with strain h because strain is the direct observable in the LISA observatory — the data streams encode the strain measured in the arms of the interferometer. As a consequence

¹⁸An observatory will detect that a binary is chirping when the binary frequency is $f > f_s$, where f_s is the *stationary frequency* defined in Eq. 46.

when working with backgrounds¹⁹ it is often useful to compute a *characteristic strain* h_c which is related to the power spectral density by

$$h_c = \sqrt{f \cdot S_h} . \quad (33)$$

This quantity is dimensionless, as is appropriate for a strain, and is independent of the LISA observation time. To make a plot of h_c for a stochastic background, one must compute the appropriate threshold sensitivity curve by evaluating Eq. 33 with $S_h(f) = (h_f^L)^2$, where h_f^L is the threshold spectral amplitude of the LISA detector defined in Eq. 8.

The key lesson to take away from these myriad of possible representations for source strength is that if the strength is to be indicated on a plot, the threshold sensitivity must match the method used to compute the strength of the source. In most instances, the fundamental quantity is the power spectral density $S_h(f)$ which presumably is known for the source, and is given by the square of Eq. 8 for the detector²⁰.

As an estimator of detectability, the *signal-to-noise ratio* (SNR) is greatly favored in gravitational wave astrophysics, as it is simple to estimate in many cases, and many important quantities scale with the SNR, such as error in parameter estimations and computational timescales for certain kinds of search algorithms.

For periodic sources, with spectral amplitude defined by Eq. 26, and given the shape of the LISA sensitivity curve, $h_f^L(f)$, the signal to noise ratio, ρ , is then estimated as

$$\rho = \frac{h_f(f)}{h_f^L(f)} = \frac{h_o \sqrt{T_{obs}}}{h_f^L(f)} . \quad (34)$$

This estimate of the SNR will not be precise in the regime where the structure of the waveform changes on timescales short compared to the observation time, or where the shape of the instrumental noise is changing rapidly as a function of frequency. For general computations, however, this simple estimator is a good “first cut” for considering the strength of sources which can be computed rapidly from simple parameters describing the system of interest.

Similar estimators can be created for other kinds of sources. For a bursting source, with maximum amplitude h_b and a width in time of τ_b , the signal will be centered at a frequency of approximately $f \simeq 1/\tau_b$. The burst will have spectral amplitude given approximately by Eq. 31 and have SNR

$$\rho = \frac{h_b \sqrt{\tau_b}}{h_f^L(f)} . \quad (35)$$

For stochastic gravitational wave backgrounds with power spectral densities $S_h(f)$, the SNR can be estimated by

$$\rho = \frac{\sqrt{S_h(f)}}{h_f^L(f)} . \quad (36)$$

Simple estimators like Eqs. 34-36 provide a quick way of reducing the problem of SNR estimation to the backs of envelopes and quick and dirty computer programs. In many scenarios, it is computationally implausible to consider computing the SNR in any other way (*e.g.*, computing the SNR for each of the 10^7 compact binaries in the galaxy). A careful practitioner should treat these estimators with care, and use them to guide calculations or as the first step in a hierarchical program which will ultimately consider a more robust estimation of the signal to noise ratio motivated by the data analysis technique of choice.

An obvious problem with these simple estimators of the SNR is they really only convey information about how strong a source is when it is at a single gravitational wave frequency f . As will be seen in Section 4, many sources in the low frequency band will be dynamically evolving on timescales which are short compared to a typical observation

¹⁹Or other broadband sources, such as sources which sweep in frequency during a LISA observation.

²⁰The spectral amplitude h_f^L (or “root spectral density”) of the detector is the default output for LISA sensitivity curves generated with the *Sensitivity Curve Generator*[23].

time. In a very real sense, making good SNR estimates depends on the evolution of the source during the observing run. An improved, but relatively simple SNR estimate is to integrate over the spectral energy distribution of the emitted gravitational waves, dE/df , weighted by the instrumental sensitivity. The SNR, averaged over all sky positions and source orientations, is defined in this case by[51]

$$\langle \rho^2 \rangle = \frac{2}{5\pi^2 D^2} \int_0^\infty df \frac{1}{f^2 S_N(f)} \frac{dE}{df}, \quad (37)$$

where D is the distance to the source²¹, and $S_N(f) = (h_f^L)^2$, where h_f^L is the sensitivity curve defined in Eq. 9 and plotted in Figure 10. This SNR is different than the estimators shown in Eqs. 34-36 in that it is integrated over all frequencies at which the source is observed, and is a *cumulative* SNR which characterizes the entire LISA observation of the source.

Different types of sources will have different spectral energy distributions. For instance, an inspiralling binary has[51, 59]

$$\frac{dE}{df} = \frac{1}{3} \pi^{2/3} \mu M^{2/3} f^{-1/3}. \quad (38)$$

The spectral energy distributions can be derived for other gravitational wave emission scenarios²², and used to compute the expected SNR for almost any desired observation scenario. More robust SNR estimates can be made when a specific data analysis procedure (*e.g.*, optimal matched filtering) is chosen, and the reader is encouraged to explore the literature on the subject for specific techniques of interest.

The SNR is of particular interest not only from the standpoint of determining whether a source is detectable, but is often a good estimator for determining errors in the estimation of astrophysical parameters. Several studies of LISA's parameter estimation capability have been carried out [48, 58, 61], and found that the errors in measured parameters scale as inverse powers of the SNR. For example, the error in LISA's ability to deduce the sky position of a source scales like

$$\Delta\Omega = \frac{\Omega_o}{\rho^2}, \quad (39)$$

where Ω_o is a scaling constant for the error determined by the various parameter estimation studies. The result embodies the intuitive notion that it is easier to determine the properties of a bright signal than a dim signal. This kind of scaling has been put to use to understand LISA's performance as an astronomical observatory in a variety of scenarios, ranging from locating globular clusters [62] to linking supermassive black hole mergers with electromagnetic observations [52]. Online tools have started to appear [63] which quickly estimate the LISA parameter errors for single sources.

4. ASTROPHYSICAL SOURCES

While the design and construction of interferometric observatories is one of the grandest endeavours in experimental science, and the proposed measurements of the minute stretching of spacetime is fantastic in the extreme, the true driving force in this new era of gravitational wave science is the promised return in our ability to probe, characterize and understand astrophysical systems.

In this section, the low-frequency gravitational wave spectrum is examined in detail, with particular attention to broad classes of sources which will be important contributors to the science LISA will illuminate. A recent review of gravitational wave sources can be found in [64].

²¹For sources at cosmological distances, the distance D is the luminosity distance $D(z)$, and the constant coefficient in front of the integral in Eq. 37 is multiplied by a redshift factor of $(1+z)^2$.

²²For instance, dE/df for the ringdown phase, after black holes collide, is given by Eq. 3.18 of [51].

4.1. Science with LISA

The science case for LISA is compelling, made strong by the fact that there are *guaranteed sources* in the low-frequency gravitational wave band, and consequently, a definitive case for the science that the observatory should be capable of returning. In the broadest strokes, the LISA science goals to understand the Universe from low-frequency gravitational wave observations can be stated in four “pillars”:

- ▷ to understand the origin and evolution of compact, massive objects with strong gravitational fields
- ▷ to understand the *evolution of populations* of compact, massive objects on scales ranging from the size of the galaxy, to the size of the known Universe
- ▷ to understand the *structure* and *evolution* of the Universe, from times shortly after the Big Bang to the present
- ▷ to probe the fundamental theory of gravity in regimes where the gravitational fields are *strong* and *dynamic*

One can think of each of these pillars by categorizing questions about the Universe. A simple and non-exhaustive list of interesting questions might be:

- ▷ *Origin and evolution of compact objects*: How do supermassive black holes form and grow? How do short period binary white dwarf systems evolve in mass and period? What kinds and ratios of stellar mass objects are captured and swallowed by supermassive black holes in galactic nuclei?
- ▷ *Evolution of populations of compact objects*: How many supermassive black hole binaries are there in the Universe? What role do stars and/or gas play in helping supermassive black hole binaries merge? How do star clusters in the centers of galaxies evolve under influence of a supermassive black hole? Are the compact stellar mass binaries in the galaxy distributed in the same way as the rest of the mass in the galaxy? What is the density of binaries in the galactic halo?
- ▷ *Structure and evolution of the Universe*: Is there a measurable spectrum of primordial gravitational waves emanating from a time prior to recombination, and if so, what are its properties? How does the redshift distribution of supermassive black hole masses correlate with the formation of large scale structure?
- ▷ *Probe the fundamental theory of gravity*: Do gravitational waves propagate at the speed of light? How many gravitational wave polarization states are there? Does the Kerr solution of general relativity really approximate an astrophysical black hole? Are there other spin fields (*e.g.*, scalar fields) in the correct fundamental theory of gravity?

These and many other questions will be answered, and new questions posed, as a consequence of observing the various objects which populate the low-frequency gravitational wave band. Our current understanding of the band can be characterized in broad taxonomical classifications, illustrated by the swaths in Figure 11 which roughly delineate the expected area signals in the band will cover. The primary players in the low frequency arena are black holes of all sizes²³, extreme mass ratio binaries where the primary mass is significantly larger than the secondary, and galactic binaries.

The rest of this section is devoted to discussion of each of these broad taxonomical areas, and the science that LISA will enable with respect to each of these sources.

²³There are three distinct populations of black holes that will be important to LISA: inspiralling and merging supermassive black hole binaries (the terms *supermassive* is used loosely, as expected masses range from $\sim 10^3 M_\odot$ to $\sim 10^9 M_\odot$), supermassive black holes which are the primary in extreme mass ratio inspirals, and stellar mass black holes which are in binary systems (either as EMRIs, or with a nearly equal mass companion).

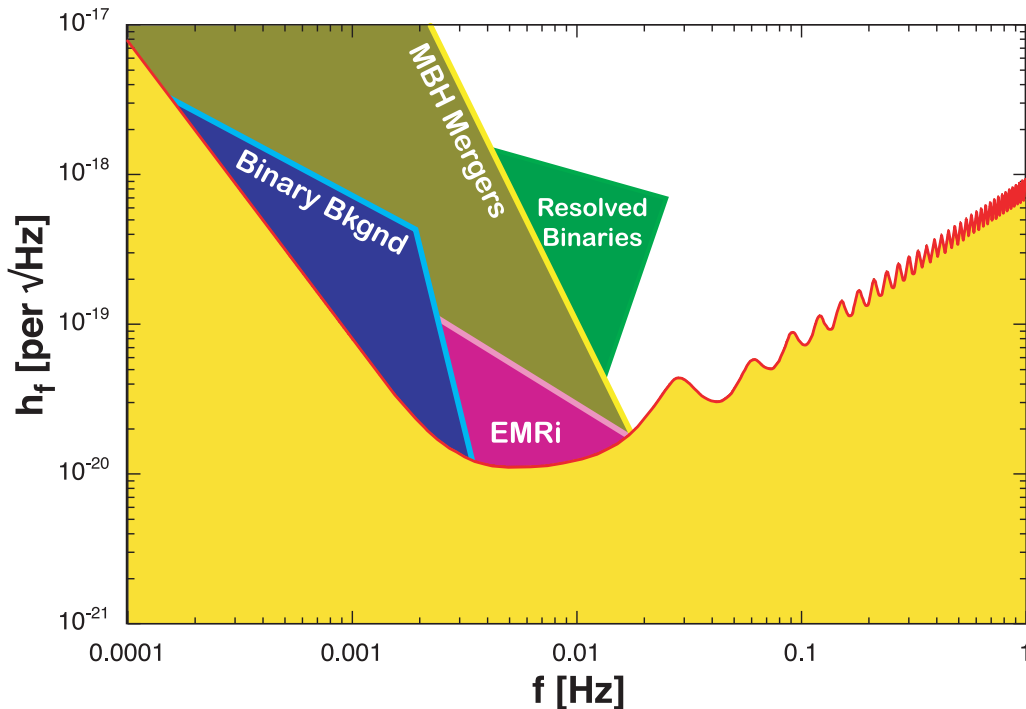


Figure 11: The LISA discovery space, delineated by the instrumental threshold corresponding to sources with $SNR = 1$. The broad areas marked indicate in a rough way what types of sources are expected to populate each region of the discovery space, as discussed at great length in § 4. Note that over much of the discovery space, the populations are *overlapping*, and data analysis procedures will need to be capable of handling this.

4.2. Compact Galactic Binaries

The low-frequency gravitational wave spectrum is alive with the background murmur of a vast population of compact short period binaries in the Milky Way galaxy. The galactic population of close binaries is largely comprised of white dwarfs, but can also include neutron stars and stellar mass black holes. Any combination of these three constituents is plausible. The overall population itself is usually considered in two categories: the *resolvable binaries*, and the *confusion foreground*. While the dominate galactic binary signal is expected to come from our own Milky Way galaxy, there is expected to be a weak confusion background of *extragalactic* binaries which may be detectable by an instrument like LISA.

Attempts to estimate the galactic gravitational wave background²⁴ have a long history, beginning with the pioneering work of Hils, Bender and Webbink (HBW) [65], who calculated the gravitational radiation incident at Earth from different binary populations distributed throughout the galaxy.

Building on the work of HBW, Hils and Bender later reconsidered the galactic background, attempting to estimate at what frequencies LISA would become *confusion limited*[66, 67] based on the theoretical abundances derived in HBW. The confusion limit is the overall amplitude, as a function of frequency, where an instrument is not able to resolve two signals in the data stream. The conventional wisdom is that if two binaries with frequencies f_1 and f_2 are not separated by more than the LISA frequency resolution, $\Delta f = 1/T_{obs}$, where T_{obs} is the LISA observation time, then they will not be individually resolvable from one another. The binaries are resolved when

$$f_1 - f_2 > \Delta f . \quad (40)$$

²⁴In some of the literature, the signal from the galactic population of close binaries is referred to as the *galactic foreground*, because the galactic sources lie between our detectors and other, more distant systems LISA will observe, such as SMBH binary mergers.

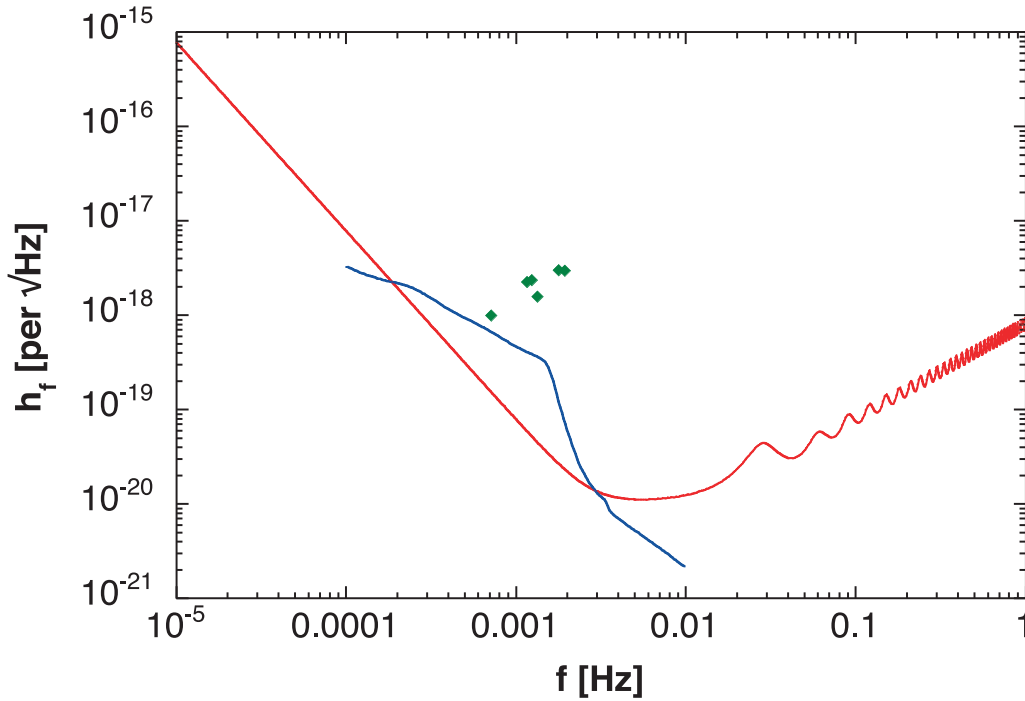


Figure 12: The classic estimate of the confusion limited galactic binary background due to Hils and Bender [67] is plotted over the standard LISA sensitivity. The solid points represent the standard estimates of the strength of the six verification binaries listed at the top of Table II (note they are somewhat higher than the values given by the simple scaling amplitude, owing to a more sophisticated treatment).

This is the LISA equivalent of the Rayleigh resolution criterion in electromagnetic astronomy, where two point sources (*e.g.*, stars) cannot be separated in an image because the resolving power of the telescope cannot “split” them. The common nomenclature in the LISA literature is that “the binaries are in the same frequency bin.”

The Hils-Bender estimate is the most common background used in the LISA literature. The background is often treated as another source of noise and merged with the instrumental sensitivity to make an effective sensitivity which is used as the baseline for data analysis studies. The background is plotted over the standard sensitivity curve in Figure 12.

More recent work on the galactic background has turned to *population synthesis*, which generates a progenitor binary population, then evolves that population forward in time to the present day, accounting for evolutionary processes that cause the mass and period distributions of the binaries to evolve. Many realizations have been generated [68–71], but these calculations show a range of predictions for the overall number of binaries in the population and as a consequence will yield different estimates of the ultimate confusion level for an instrument like LISA. What the ultimate confusion limit is depends on the overall number of binaries in the galactic population, and the identification and subtraction algorithms²⁵, which remove *individually resolvable* systems from the data stream.

The abundance of compact white dwarf binaries in the galaxy, characterized most often as a value for the local space density, is the largest single uncertainty in determining what the overall level of the galactic confusion background will be. Early searches for short period white dwarf binaries did not recover any systems [72]. Surveys in the mid-1990s began to detect a few systems [73, 74], and more recently the SPY (*Supernova Ia Progenitor surveY*) project has undertaken an extensive program to spectroscopically survey 1500 white dwarfs, resulting in the discovery of many binaries of potential interest (*e.g.*, [75, 76]) for characterizing the low frequency background. Never-the-less,

²⁵Like gCLEAN, discussed later in this section.

uncertainties still exist in characterizing selection effects in surveys for close white dwarf systems, and this impacts the ability to convert new observations into useful numbers on abundances which can be effectively used to predict the character of the low frequency gravitational wave background. A range of predicted levels can be seen in the various population synthesis models. Hils and Bender [66] opted to show two curves for their background estimate: the 100% curve derived directly from the HBW abundances, and a more optimistic 10% curve, reduced from the full curve. The 10% has almost uniformly become the default in the LISA literature, and is what is shown in Figure 12²⁶. When surveying the LISA literature, care should be taken to note whether estimates and simulations of the background which build upon the previous work of HBW or Hils and Bender include the 100% or 10% populations. Readers who are interested in the galactic background, or are seeking to include the effects of the background in their research should be aware of the overall uncertainty and consider the implications of this uncertainty when drawing conclusions about their results.

An often useful quantity when working with the background is the density of sources in frequency space, dN/df . A common value is

$$\frac{dN}{df} = \eta_o f^{-11/3}, \quad (41)$$

The value of the constant η_o is determined by the number of binaries, N_* , in the frequency band of interest:

$$N_* = \int_{f_1}^{f_2} df \frac{dN}{df}. \quad (42)$$

A good value for the scaling constant is $\eta_o = 2 \times 10^{-3}$ [77, 78], and using this scaling in Eq. 42 in the LISA band from $f_1 = 10^{-4}$ Hz to $f_2 = 0.1$ Hz, one finds $N_* = 3.5 \times 10^7$ close binaries, in good agreement with expectations. In principle, a value for η_o should be worked out for *every* background realization, but this form is often adopted and useful in many scenarios. As an example, one can make a rudimentary estimate of the frequency where the number of binaries in a LISA frequency bin is $N_* = 1$ and sources in the binary background become individually resolvable. To do this, set $f_1 = f_o$ and $f_2 = f_o + \Delta f$ in Eq. 42. This yields:

$$\begin{aligned} N_* &= \int_{f_o}^{f_o + \Delta f} df (dN/df) \\ &= \eta_o \cdot \frac{3}{8} f_o^{-8/3} \left[1 - \left(1 + \frac{\Delta f}{f_o} \right)^{-8/3} \right] \\ &\simeq \eta_o f_o^{-11/3} \Delta f, \end{aligned} \quad (43)$$

where the last step has employed the approximation $\Delta f \ll f_o$. Setting $N_* = 1$, one can solve for f_o :

$$f_o = \left[\frac{\eta_o \Delta f}{N_*} \right]^{3/11} = 1.6 \text{ mHz}. \quad (44)$$

Above this frequency, the occupation number of a single LISA frequency bin is generally less than 1 for $T_{obs} \sim 1$ yr. The exact frequency at which the background transitions from being confusion limited to individually resolved sources depends on the exact character of the background, the total observing time²⁷ T_{obs} , and the data analysis procedure being used to identify sources. The exact point at which the transition occurs is the subject of much research [79], but a good rule of thumb to account for all these mitigating issues is to take the *confusion frequency* to be $f_o \simeq 3$ mHz.

Individually resolved sources will be found in the low-frequency band in two types. The first type are binaries which exist at frequencies above the confusion frequency, $f \gtrsim f_o$. In this regime, the density of binaries (*e.g.*, as given by

²⁶The curve shown in Figure 12 is the 10% curve with the additional population of cataclysmic variables described in [67].

²⁷Remember that the observing time sets the LISA frequency resolution, $\Delta f = 1/T_{obs}$.

Table II: LISA Verification Binaries. There are many compact galactic binaries, close to the Earth, which have been studied electromagnetically and parameters are known well enough to predict that they will be *guaranteed* LISA sources, visible very soon after the observatory begins operations. These six binaries are generally known as the *verification binaries*, and are the most well understood. Physical data is from [80], and periods are from NSSDC catalog 5509 [81].

Name	RA (J2000.0)	DEC (J2000.0)	Orbital Period (s)	Distance (pc)	$m_1(M_\odot)$	$m_2(M_\odot)$	h_o
AM CVn	12h 34m 54.58s	+37d 37m 43.4s	1028.73	101	0.5	0.044	1.24×10^{-22}
HP Lib	15h 35m 53.165s	-14d 13m 11.51s	1118.88	165	0.6	~ 0.03	5.57×10^{-23}
GP Com	13h 05m 43.44s	+18d 01m 02.2s	2791.58	165	0.5	~ 0.02	1.79×10^{-23}
V803 Cen	13h 23m 44.54s	-41d 44m 32.1s	1611.36	~ 100	0.6	~ 0.02	4.83×10^{-23}
CR Boo	13h 48m 55.39s	+07d 57m 30.6s	1471.31	157	0.6	~ 0.03	4.88×10^{-23}
CP Eri	03h 10m 32.83s	-09d 45m 06.2s	1723.68	~ 100	0.6	~ 0.02	4.62×10^{-23}

Eq. 41) is less than one binary per frequency bin, and the binaries do not overlap with one another²⁸. In this regime, any galactic binary is individually resolvable as long as it is strong enough to be seen over the instrumental noise of the observatory. The second type, binaries at gravitational wave frequencies less than the confusion frequency, $f \lesssim f_o$, are in a regime where Eq. 41 predicts that the occupation number of a LISA frequency resolution bin is greater than one²⁹. These binaries are individually resolvable only if they are strong enough to be seen *above* the composite noise spectrum of the instrument and galactic confusion background.

The individually resolvable galactic binaries are important for many reasons. The ability to resolve an isolated compact binary should allow the study of the structure of the component white dwarfs, as well as tidal interactions between the two bodies in the compact binary. This can have important implications for our understanding of doubly degenerate progenitors of Type Ia supernovae, as well as providing a galaxy wide probe of a highly evolved stellar population. The easiest parameter to extract from each of the individual detections will be the gravitational wave frequency, which is directly related to the orbital period. Therefore the detection of a resolved population will provide a direct probe of the period distribution of the compact binaries in the galaxy. Additionally, a group of well studied binaries which are known in advance of LISA’s launch will also provide an opportunity to test and validate data analysis and subtraction procedures immediately after the observatory’s “first wave”³⁰.

Estimates suggest that LISA should be capable of resolving ~ 5000 to $\sim 10,000$ individual binaries, distributed throughout the entire galaxy. Among these systems will be a set of known *verification binaries*. The verification binaries are individually resolvable systems which have been well studied and characterized through electromagnetic observations. Table II lists the location and known properties of several of the verification binaries which are currently known.

The search for other LISA resolvable systems is an ongoing endeavour. Extensive archived observational data exists (*e.g.* [82]), a fact which has been exploited to estimate LISA’s sensitivity to known cataclysmic variables [83]. New binaries which could potentially be very important to LISA are also being discovered in large photometric and spectroscopic data sets, such as the Sloan Digital Sky Survey [84]. It is important to note that while many verification binaries are currently known, a complete sample of bright binaries which span the entire LISA science band does not yet exist; such a population would be useful before the observatory launches.

Mass transferring (“interacting”) white dwarf binaries are also an important source which will radiate strongly in

²⁸The orbital motion of a detector around the Sun will cause a binary signal to spread in frequency by an amount $(\Delta f/f) \simeq v/c \simeq 9.94 \times 10^{-5}$. The implicit assumption made when considering resolvable binaries is that a suitable *demodulation* of the received signals from any given direction on the sky has been performed, and the frequency spectrum of the binary is simply that which would be seen by an observer at the solar system barycenter.

²⁹This is true even in the demodulated, barycentric spectrum.

³⁰*First wave* is a term analogous to the electromagnetic tradition of *first light*, when a new telescope’s mirror is first exposed to starlight, only in LISA’s case it will be first exposure to gravitational waves. Some gravitational wave astronomers employ the nomenclature “first light” to refer to the first time laser light is passed down the arms of an interferometric observatory.

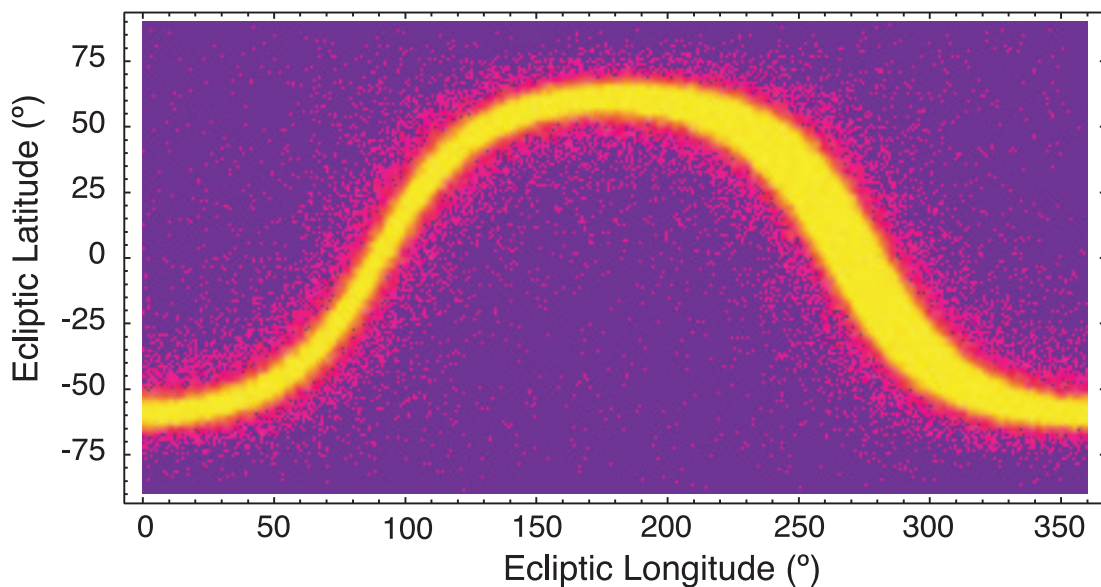


Figure 13: The number density of close galactic binaries as a function of sky position, plotted in ecliptic coordinates, based on the population synthesis models of [70].

the LISA band. LISA will be able to identify more interacting white dwarf binaries than any previous survey, and will not be biased toward those close to the Earth – they will be visible throughout the entire galaxy. Characteristics of mass transferring binaries should easily be seen in gravitational wave data. Early in inspiral phase, when the binaries are still detached, it is likely tidal effects become important and provide a mechanism for the transfer of angular momentum and energy which will modify the predicted inspiral (“chirp”) due to gravitational wave emission alone; it is unclear whether this effect will be detectable or simply produce a bias which affects our understanding of the $\{f, \dot{f}\}$ distribution function for these binaries. When the binaries come close enough together, the lower-mass companion will fill its Roche lobe and begin to transfer mass. Direct mass transfer in compact degenerate systems such as this, on long time scales, transfers angular momentum to the orbit and causes the binary system to *expand* over time. A gravitational wave observatory monitoring the evolution of the frequency would then see a *negative* \dot{f} , or *inverse chirp*, as the system evolves to longer orbital periods (lower gravitational wave frequency). Because common detection strategies amount to very sensitive monitoring of the received gravitational wave phase, which is intimately tied to the orbital phase of the binary, observations by LISA should provide a sensitive probe to the evolutionary process in these types of interacting binary systems.

One of the most important questions in LISA data analysis is how to identify the individually resolvable sources, and whether or not it is possible to “subtract” those sources out of the data stream, leaving behind the signals from other astrophysical systems. The problem is fraught with difficulties associated with how to disentangle sources which are strongly overlapping in the LISA data. A few techniques [85, 86] have proposed some basic techniques and shown some early successes. The problem is still, however, largely unresolved and in need of more attention.

In much of the LISA literature, the confusion background is characterized as a source of noise which must be accounted for when considering observations of other sources of gravitational waves. It is a sad fact that most often thought of *as noise*, a nuisance which interferes with seeing more interesting sources of gravitational waves (like supermassive black hole binaries or extreme mass ratio inspirals). In reality, however, the galactic binary background is an important astrophysical signal which will be easily visible to LISA and have profound implications for our understanding of the galaxy.

Studies of how to mitigate the background often exploit its character, particularly the fact that it will be anisotropically distributed on the sky, following the plane of the galaxy. A typical distribution of the number density of galactic binaries on the sky is shown in Figure 13[70]. This anisotropic distribution, coupled with LISA’s orbital motion will

modulate the signal from the background, a fact which can be exploited to determine the underlying characteristics of the binary population [71, 87].

As tracers of galactic structure, binary populations will provide observational access to many different components of the galaxy, including the disk and bulge [88], the dark galactic halo [89–91], and even globular cluster systems [62]. Observations of the galactic binary foreground in gravitational waves provide a key way to measure the properties of an assumed but unseen component of the galactic stellar population. The total population of highly evolved compact binaries provides a unique record of galactic stellar evolution which should be easily accessible to an instrument like LISA. Near the frequencies where LISA is most sensitive, it is also plausible that galactic binary signals from the Milky Way’s nearest companions might also be detected, and that there will be a low level confusion background of all the galactic binaries in the local Universe [92], which would form an ultimate noise floor in the low frequency gravitational wave band.

4.3. Supermassive Black Hole Binaries

Perhaps the strongest sources of low frequency gravitational waves will be merging supermassive black hole (SMBH) binaries. The rate at which SMBH binaries merge in the Universe is uncertain at best, but they will be detectable by LISA to extremely large distances, probing an enormous volume of the visible Universe. The detection of *any* SMBH mergers, even at a low rate, will produce interesting astrophysical results.

Most expectations are that supermassive black hole binaries should be circularized by the time their evolution is dominated by the emission of gravitational radiation, and so the equations in § 3.2 can be exploited to good effect when making back of the envelope computations about these systems. One can easily predict what black hole binaries LISA will be sensitive to by simple application of Eq. 20. Setting the frequency to $f = 10^{-4}$ Hz, near the lower edge of the LISA science band, and solving for the mass yields:

$$M_t = 10^5 M_\odot \left(\frac{41 \text{mHz}}{f_c} \right) = 4 \times 10^7 M_\odot . \quad (45)$$

This is approximately the total mass of the most massive binary that will coalesce in the LISA band. Such a binary will spend almost *no time* in the band, but less massive binaries will radiate at LISA frequencies for an extended period of time. Figure 14 illustrates this, showing the total time an equal mass SMBH binary spends in the LISA band if it is evolving by emission of gravitational radiation alone. The figure was computed from Eq. 15 by integrating from the lower edge of the LISA band³¹ ($f_1 = 10^{-5}$ Hz) up to the high edge of the LISA band ($f_2 \simeq 1$ Hz) or to the merger frequency ($f_2 = f_c$), whichever is lowest. Note that this figure makes *no account* of whether the SMBH binary will be *detectable* by LISA, only whether the frequency of the emitted waves fall within the LISA band.

Figure 15 shows the time to coalescence for a black hole system as a function of frequency, demonstrating that a wide range of black hole binaries will *chirp* significantly while in the LISA band. Whether or not a binary will be characterized as chirping in the observational data depends on the length of the observation T_{obs} , which ultimately sets the frequency resolution of the data, $\Delta f = 1/T_{obs}$. A simple conservative criterion for detecting the chirp of a binary system is that its frequency f_2 at the end of the observation is $f_2 \gtrsim f_1 + \Delta f$. The frequency at which a binary crosses a frequency bin in exactly the observation time is called the *stationary frequency*, f_s , and is computed from Eq. 15 by setting $\Delta t = T_{obs}$ and $f_2 = f_1 + \Delta f$, then solving for $f_1 = f_s$, yielding

$$f_s \simeq \left[\frac{8}{3} \frac{\kappa}{T_{obs}^2} \right]^{3/11} . \quad (46)$$

³¹Note that the precise frequency which defines the lower edge of the LISA band is currently unspecified in the LISA literature. It is widely expected that there will be a *low frequency cutoff* imposed by the instrumentation, but the cutoff frequency f_x has yet to be fixed for two reasons. First, it is unknown exactly what science will be lost as a function of the value of f_x . Second, it is unknown precisely what instrumental noises will be dominant at those frequencies, how large they will be, and whether it is possible to control them or not. A conservative estimate often used is that the cutoff will be located at $f_x \simeq 3 \times 10^{-5}$ Hz.

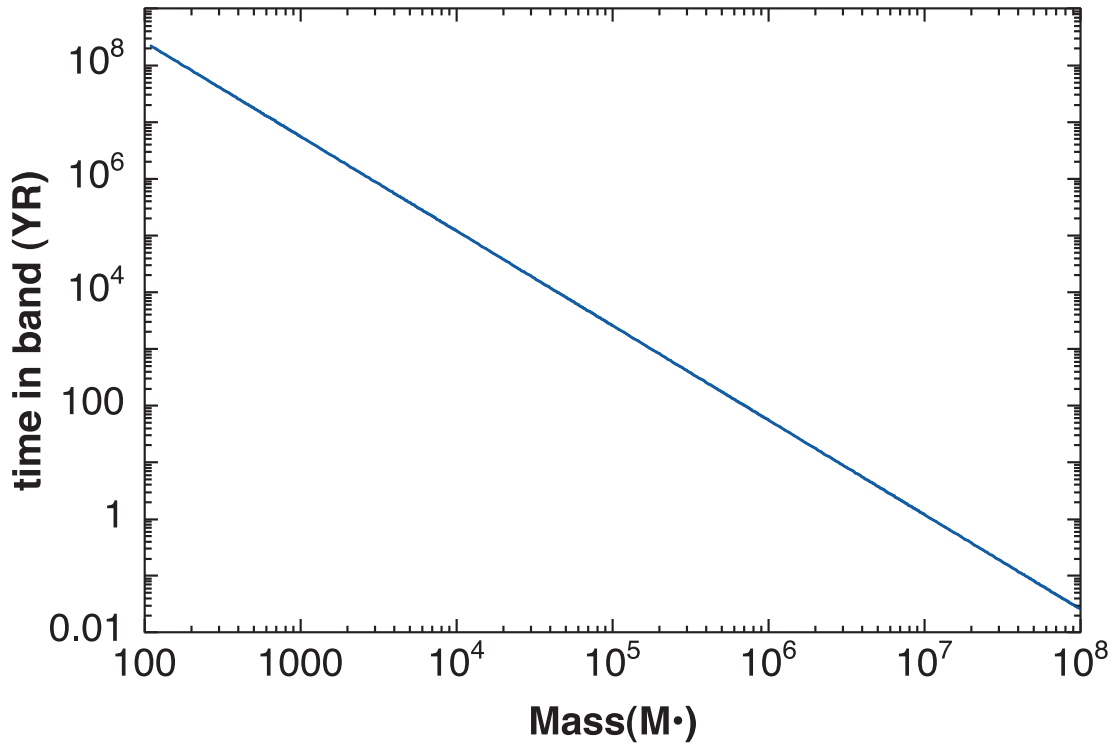


Figure 14: An approximate estimate of the time a supermassive black hole binary with masses $m_1 = m_2 = M_\bullet$ radiates in the LISA frequency band, $10^{-5}\text{Hz} \lesssim f \lesssim 1\text{Hz}$. Whether such a binary is actually visible to LISA will depend on the specifics of the source location, distance, and orientation with respect to the observatory. Note that if the computation is cutoff at the proposed cutoff frequency, $f_x \simeq 3 \times 10^{-5}$ Hz, the most massive binaries will not be accessible to LISA (*i.e.*, they will spend no time in band).

For all frequencies above this, $f > f_s$, the binary chirps by Δf in less than the observation time. Here, the approximation has been made that $\Delta f \ll f_1$, a reasonable assumption for year long observations in the LISA band. In Table III, stationary frequency f_s is shown for $T_{obs} = 1$ year and $T_{obs} = 3$ year as a function of the black hole mass $M_\bullet = m_1 = m_2$.

Given that LISA will be sensitive to supermassive black hole binaries, there is considerable interest in understanding the expected population of such systems in the Universe. These efforts serve two purposes: first, they allow LISA designers to estimate what the observatory's detection capabilities will be, and second they enable astronomers to better understand how low frequency gravitational wave observations can be used to constrain our knowledge about the assembly of supermassive black holes and the role they play in the formation of large scale structure.

Many of the expectations about the population of supermassive black holes in the Universe derives from observa-

Table III: The stationary frequencies, f_s given by Eq. 46 as a function of black hole mass $m_1 = m_2 = M_\bullet$.

$M_\bullet (M_\odot)$	$f_s (T_{obs} = 1\text{yr})$	$f_s (T_{obs} = 3\text{yr})$
10^3	1.88×10^{-3} Hz	1.03×10^{-3} Hz
10^4	6.60×10^{-5} Hz	3.63×10^{-5} Hz
10^5	2.32×10^{-5} Hz	1.27×10^{-5} Hz
10^6	8.14×10^{-6} Hz	4.47×10^{-6} Hz
10^7	2.86×10^{-6} Hz	1.57×10^{-6} Hz
10^8	1.00×10^{-6} Hz	5.51×10^{-7} Hz

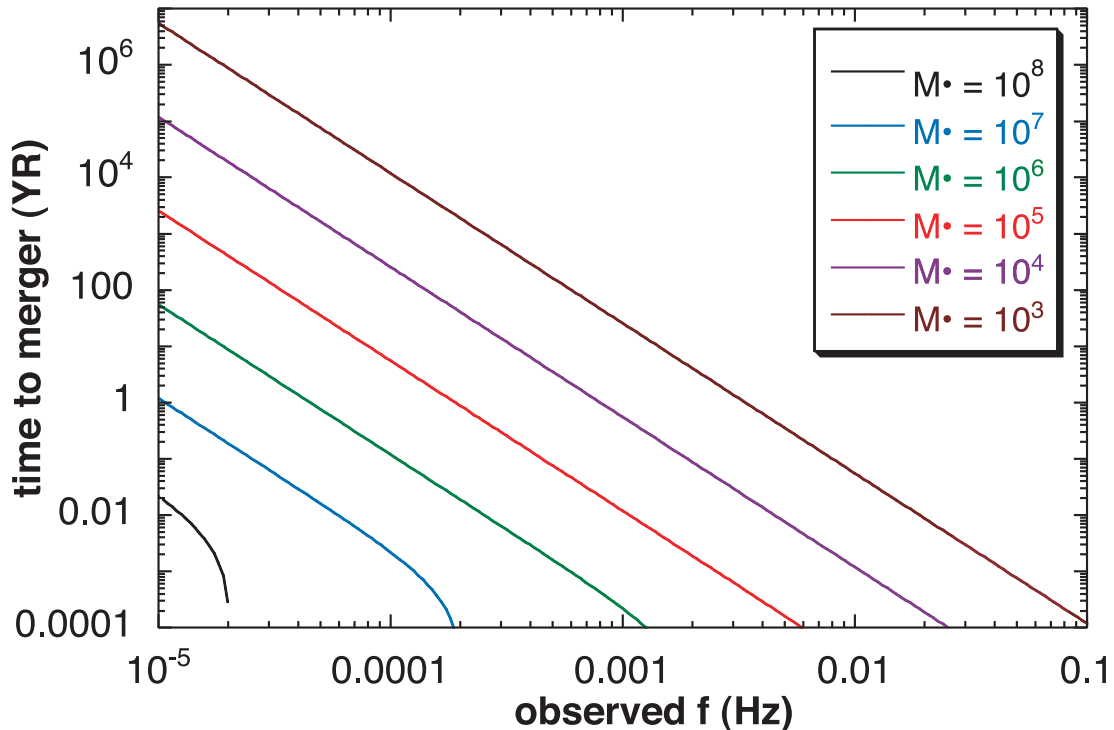


Figure 15: An estimate of the time to coalescence for a supermassive black hole binary with masses $m_1 = m_2 = M_\bullet$, as a function of observed frequency.

tions of the high redshift quasar population [93–95] which suggest that a large population of black holes has existed since early epochs. The shape of the quasar luminosity function suggests that large black holes ($M_\bullet \sim 10^5 M_\odot$) had to exist at redshifts of $z \sim 10$ in order to explain the quasar activity seen at much lower redshifts. The local census of massive black holes has been growing in recent years, driven by a growing body of observational evidence linking the mass of supermassive black holes with observational properties of their host galaxies. Early studies revealed a rough correlation between black hole mass and the bulge luminosity of the host galaxy [96, 97]. A much stronger correlation was later discovered between the black hole mass and the stellar velocity dispersion in the galactic core, the so-called “ $M\sigma$ ” relation [98–100]. The current best fit to the $M\sigma$ relation is [101, 102]

$$\log\left(\frac{M_\bullet}{M_\odot}\right) = \alpha + \beta \log\left(\frac{\sigma}{\sigma_o}\right), \quad (47)$$

where $\alpha = 8.13 \pm 0.06$, $\beta = 4.02 \pm 0.32$, and $\sigma_o = 200 \text{ km/s}$. The observational data supporting the $M\sigma$ relation currently spans from $\sim 10^6 M_\odot$ to $\sim 10^9 M_\odot$. Attempts to extend the observational link into the regime of *intermediate black hole holes* (IMBH), with masses of $\sim 10^2 M_\odot$ to $\sim 10^4 M_\odot$, have focused on looking in the cores of globular clusters [103–106]. The early evidence was limited and circumspect, but more recent observations are more sensitive, and firmly on the road to exploring the conformity of the $M\sigma$ relation in this mass regime [107].

The $M\sigma$ correlation is strong enough that it has been exploited to good effect to predict the overall census of massive black holes in the Universe [108]. The characteristics of this population will have important implications for understanding the LISA data; more importantly, the low frequency gravitational wave data will be a direct probe of the number and mass distribution functions of the supermassive black hole population, and will provide an observational baseline against which studies like [108] may be compared and constrained.

Despite our growing knowledge about the population of single supermassive black holes, it is important to keep in mind that LISA will not be sensitive to isolated supermassive black holes. The appellation to the growing evidence of single supermassive black holes grows from the fact that the base population of singles underpins the rates of *extreme mass ratio inspirals* (EMRIs, discussed in § 4.4) as well as the rate of supermassive binary mergers. The

overall merger rates detectable by LISA are the subject of much attention [109–111], with estimates ranging from 10 to nearly 100 per LISA observation time.

One of the first questions which can be addressed by a LISA detection of a SMBH binary population is how supermassive black holes grow and evolve. One the leading propositions is that black holes play a part in the formation of large scale structure, and grow in a hierarchical way, with large black holes growing from the merger of smaller black holes from early cosmological epochs [112–114]. The rate of mergers detected by LISA will yield clues to how often black holes encounter each other, the mass determination will yield clues to the overall structure of merger tree, yielding branching ratios for different processes involved in supermassive black hole assembly and extending our understanding of the evolution of structure in the Universe [115].

Additionally, the determination of luminosity distance will fix how black hole formation proceeds in relation to the formation of large scale structures in the Universe. In this modern era of high precision cosmology, our knowledge of the parameters which characterize the cosmological model will allow the use of low frequency gravitational wave observations to probe the mass and merger history of the supermassive black hole population as a function of redshift [116].

While population probes are an important aspect of our understanding of how supermassive black holes grow and evolve, gravitational wave observations will also directly probe the character of the black holes themselves, on scales comparable to the size of the event horizons. How the information about the black hole (like spin and mass) is encoded in the waveform is a topic of much focused research (for reviews, see [117, 118]). Recent progress in attempts to simulate the late stages of binary black hole inspiral [119, 120] hold the promise of providing accurate waveforms which can be used to detect and characterize SMBH waveforms in the LISA data stream. Once inspirals can be reliably simulated, attention will turn to the merger phase and connecting behaviour of the system between the final plunge and the late stages of the black hole ringdown.

Additionally, once the encoding of the astrophysical parameters in the gravitational waveforms is understood, data analysis procedures must be able to *extract* that information from the received waves. The development of extraction procedures is often entangled with studies of *parameter estimation* which seek to characterize how well LISA will be able to determine the physical description of the supermassive black hole binary. An early comprehensive study [48] considered LISA determination of sky location, luminosity distance and mass of SMBH systems by including a simple model of LISA’s orbital motion around the Sun. Later studies [58] also considered the angular resolution of detectors in *precessing plane* configurations like LISA’s, as well as *ecliptic plane* interferometers which remain flat in the ecliptic plane as they orbit the Sun. More recent studies [61] have included spin effects to the binary black hole waveforms and looked at the effect on LISA’s parameter estimation ability. Other similar studies have examined the problem in the context of constraining alternative theories of gravity [121, 122].

These kinds of parameter estimation studies are important, not only for exploring LISA’s ability to extract fundamental information about the structure and theory of black holes, but also because they embody the quality of information that will be available to astrophysicists for the phenomenological exploration of the *astrophysical character* of black hole systems. Of particular interest is the coevolution of the spins of the black holes and the final spin after the merger remnant settles down to a quiescent state [123], which gravitational wave observations should be able to shed some light on.

Much of the binary SMBH literature is dominated by estimates of merger rates and how to compute inspiral waveforms, which are all important issues for LISA data analysis. However, it is important to remember that for every observed merger of an SMBH binary, there is going to be a ringdown signal which will almost certainly be visible to LISA. Simple estimates of the SNR for inspiral and ringdown events (*e.g.*, following the techniques outlined in [51], but using an updated LISA sensitivity curve [23]) can easily show that for very modest SMBH masses, the ringdown waves very likely will have higher SNR than the inspiral waves themselves, as shown in Figure 16.

The post-merger waveforms will provide a detailed probe of the strong field dynamics which govern the evolution of the highly distorted merger product as it settles down into a quiescent black hole state. While the late stages of ringdown are adequately understood from perturbation theory as the superposition of the quasi-normal modes of the black hole, the early ringdown behaviour immediately after the binary merger phase is less well understood, largely

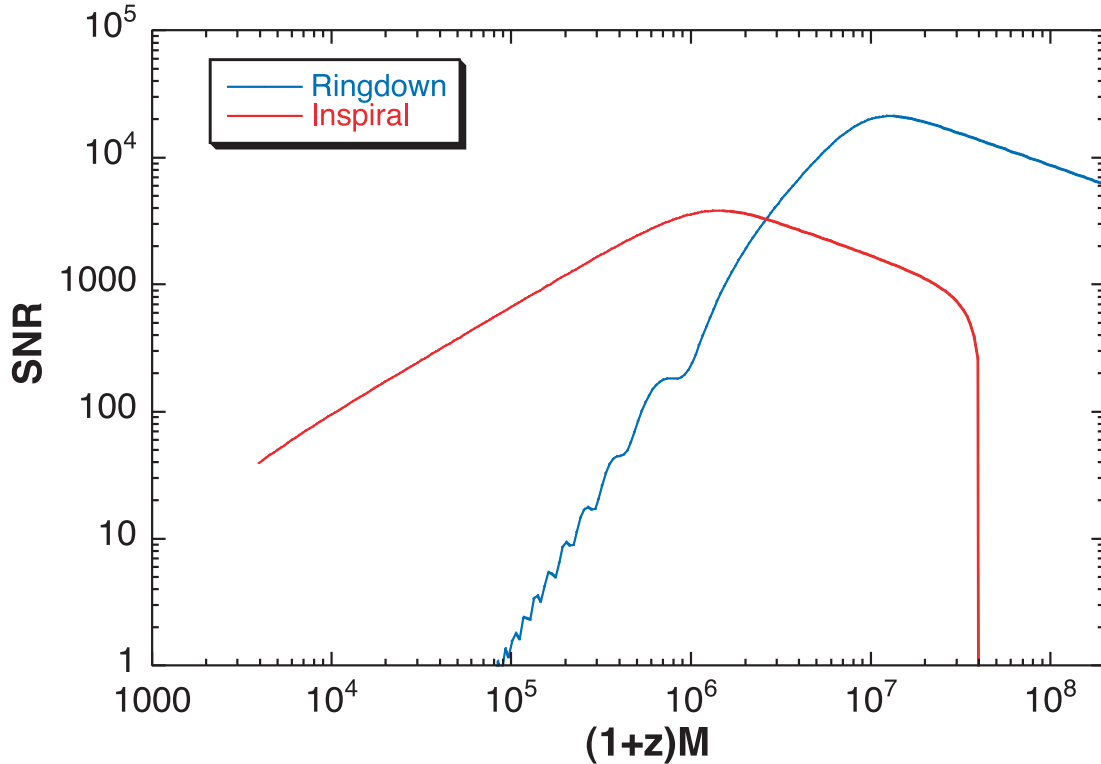


Figure 16: Comparative signal to noise ratios, as a function of black hole mass M , for the last year of inspiral of an equal mass SMBH binary as well as the ringdown after the merger of the system. The method and ringdown description used to generate this figure follows that of [51], updated to use a modern LISA sensitivity curve [23] with a low frequency cutoff of $f = 1 \times 10^{-4}$ Hz, and for a redshift of $z = 1$ in a modern cosmology (for $z = 1$ the luminosity distance is $D_L = 6.6$ Gpc [124]). Note that for black hole masses larger than $M \sim 10^6 M_\odot$ the SNR measured from the ringdown can be larger than the SNR from the last year of inspiral.

due to uncertainties about how much energy is input into the ringdown and what normal modes are excited in the initial ringdown data. These issues are particularly important because the initial data characterizes the non-linear dynamics which couple different normal modes in the excited black hole state. For a comprehensive review of black hole ringdown, see [125].

4.4. Extreme Mass Ratio Inspirals

It is widely expected that supermassive black holes in galactic nuclei will, on occasion, capture and merge with stellar mass objects [126]. These capture and inspiral events are called *extreme mass ratio inspirals* (EMRIs), and are of vital interests to both gravitational theorists and astrophysicists. The phenomenology of EMRI waveforms is only beginning to be probed, but the detected waves should carry information about the structure of the supermassive black hole spacetime. The expectation is that EMRIs will be detectable out to redshifts $z \sim 1$; the detection of even a handful of these events will probe the dynamics and evolution of nuclear star clusters in the centers of galaxies.

EMRI studies are rooted in attempts to understand the interactions between supermassive black holes and the dense stellar clusters which surround them. These studies are typically large numerical simulations, either large N-body simulations [127–129] or Monte-Carlo methods [130–132] which are based on an early techniques proposed by Hénon for study of globular cluster systems [133]. The aspect of these simulations which is of interest to gravitational wave astronomy is the long time evolution of the stellar clusters and the times when cluster members come close to the black hole or are absorbed by it.

The primary quantity underpinning studies of EMRIs relating to LISA is the rate of detectable inspirals. The

uncertainties associated with the precise stellar distributions around supermassive black holes makes the predictions of overall EMRI rates highly uncertain as well. Studies of the inspiral rate are often tied to descriptions of the *loss cone* [134, 135] which is the region of orbital angular momentum and energy phase space where stars have a high likelihood of becoming permanently bound to the black hole and ultimately lost from the cluster by orbital decay through the emission of gravitational radiation.

Observational clues to the overall propensity of EMRIs in the Universe can be found from observations of our own Milky Way galaxy. Long term monitoring of the region near the black at the center of the Milky Way³² in the infrared has yielded long baselines in the time evolution of a cluster of stars that have pericenters which pass very close to the black hole [136, 137]. The cluster has been observed long enough that curvature can be seen on many of the stellar trajectories, and as a consequence, good orbital parameters can be determined. Additionally, the orbits yield a good measurement of the black hole mass, which is currently taken to be $M_{\bullet} = 3.7 \times 10^6 M_{\odot}$ [137, 138]. For stars which have made the closest observed approach to the black hole (the stars known as SO-2 and SO-16 have each passed within ~ 50 AU of the black hole), one can estimate the strength of the gravitational radiation during the pericenter passage; while it is strong, it is at low enough frequency that it would be well below the detection capabilities of an instrument like LISA. Never the less, the fact that there are known stars which come close to the central black hole can be exploited, and the known orbital parameters used to calibrate models which seek to describe entire populations, including not only infrared luminous stars that can be electromagnetically observed from Earth, but also dim, compact stellar remnants like white dwarfs, neutron stars and stellar mass black holes. This plan has been illustrated to good effect to predict the rate of EMRIs in the Milky Way galaxy [139].

The predicted EMRI rates for the Milky Way form the basis of the overall predictions from the integrated EMRI rate in the LISA band over the entire volume accessible to the observatory [78]. Other factors which influence the detectability of an EMRI are the total length of a LISA observation T_{obs} , and the overall performance factor of the data analysis pipeline which removes other source signals which are competing with the EMRIs. Table IV shows the predicted detectable EMRI rates from [78] for both optimistic and pessimistic scenarios.

A particularly interesting feature that is expected to be observable in EMRI orbits is *zoom-whirl* behaviour [140]. In conventional Keplerian orbital dynamics it is common to characterize particle motion in terms of a single orbital frequency, associated with the orbital period. For general motion around black holes, it is possible to have three characteristic frequencies associated with the periods for radial motion, azimuthal motion, and polar motion. In general, these three frequencies do not have to be commensurate, and if the particle orbit passes close to the black

Table IV: Number of EMRI detections. The predicted number of detectable EMRIs by LISA for pessimistic mission scenarios (3 year mission, poor data analysis) and optimistic mission scenarios (5 year mission, good data analysis). The first two columns are the black hole mass M_{\bullet} and the compact body mass m_2 . Table from original data in [78].

$M_{\bullet}(M_{\odot})$	$m_2(M_{\odot})$	Optimistic #	Pessimistic #
3×10^5	0.6	8	0.7
3×10^5	10	700	89
3×10^5	100	1	1
1×10^6	0.6	94	9
1×10^6	10	1100	660
1×10^6	100	1	1
3×10^6	0.6	67	2
3×10^6	10	1700	134
3×10^6	100	2	1

³²The central black hole in the Milky Way is coincident with the bright radio source known as *Sagittarius A**.

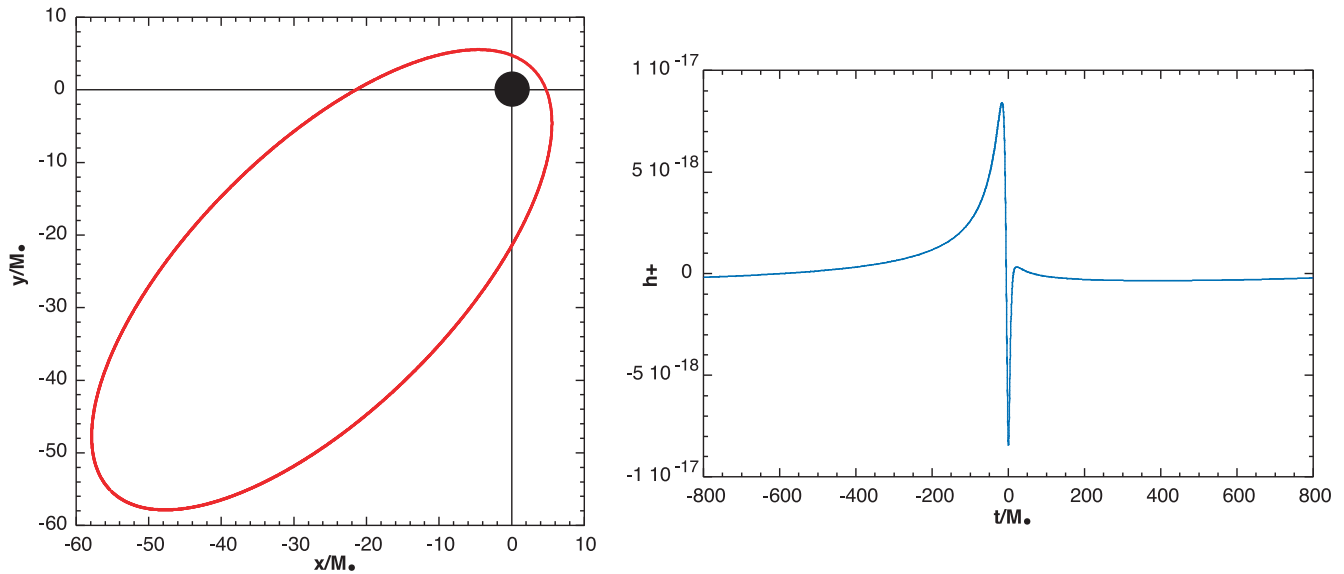


Figure 17: The left panel shows a Keplerian orbit of a stellar mass body around a supermassive black hole. The right panel shows the gravitational waveform associated with this orbit. Note the localized burst of radiation, which is generated when the small body passes through periaapsis.

hole the differences can be extreme. For example, consider a purely equatorial orbit. On close passes by the black hole, it is possible for the total advance in the azimuthal phase of the orbit, $\Delta\phi$, to be greater than 2π during any given radial period (*i.e.*, the time between apocenter passages). Similarly, for inclined orbits, the particle will oscillate back and forth across the equatorial plane more than once for each radial period.

Figures 17 and 18 show two example orbits around a Schwarzschild (non-spinning) black hole, and the effect of the zoom-whirl behaviour on the gravitational waveforms. In Figure 17, the particle does not whirl, and the pericenter passage produces a single strong burst of radiation. In Figure 18 the Keplerian orbit has been replaced with the true geodesic orbit around the black hole, and the orbit whirls near the pericenter passage, having a profound impact on the structure of the waveform. In both cases, the orbits are chosen to have the same orbital parameters, to explicitly illustrate the difference between using Keplerian orbits and true geodesic orbits.

These orbits, while apparently extremely non-intuitive, are not exotic in any way. They are simply manifesting an extreme form of perihelion precession, a well understood phenomenon in general relativity. An easy way to understand the extreme nature of the particle motion when it is near the black hole is to consider the motion of the small body in the effective potential of the black hole, as shown in Figure 19. The energy of the particle fixes its relationship to the potential, and its motion oscillates between the inner and outer turning points of its orbit, where the total energy of the star coincides with the level of the effective potential. In the case shown in the figure, the inner turning point (pericenter) is very close to the radius of the local maximum of the potential located at $r = r_{uco}$, which is defined in terms of the orbital eccentricity³³ by [55]

$$r_{uco} = 2M_{\bullet} \frac{3+e}{1+e}. \quad (48)$$

When the star approaches its pericenter, which very nearly coincides with r_{uco} , its instantaneous parameters are very similar to that of a purely circular orbit which sits at the peak of the local maximum.

³³The usual habit when describing orbits in terms of effective potentials is to work with the orbital constants of motion, $\{E, L\}$. There is a direct mapping between these conventional constants and the geometric parameters, $\{r_p, e\}$, which characterize the orbit, and are often more convenient to work with. For details, see [55].

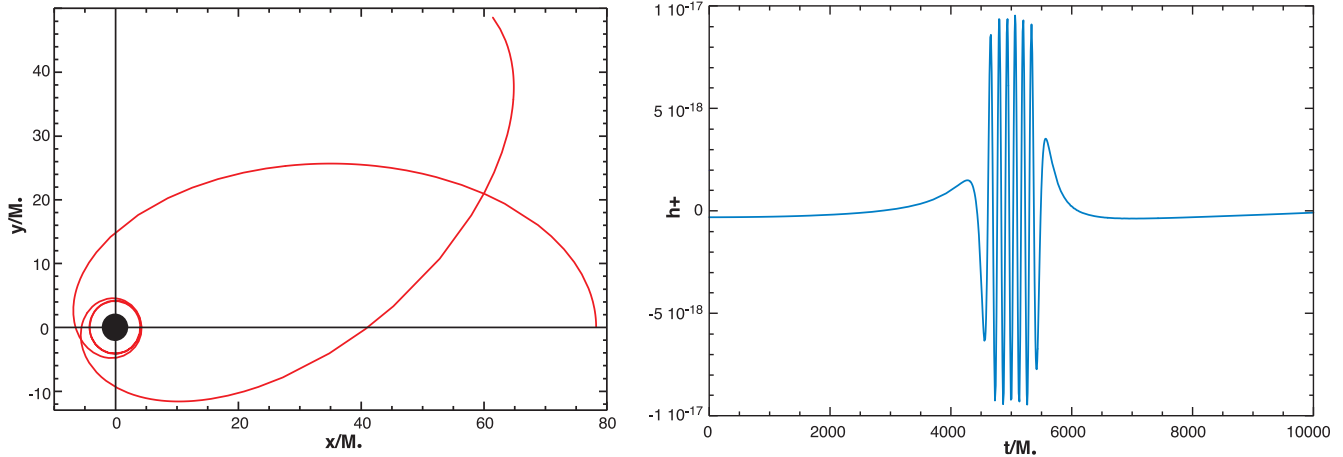


Figure 18: The left panel shows an orbit of a stellar mass body around a supermassive black hole, with the same pericenter orientation and orbital parameters as the orbit shown in Figure 17. In this figure, however, the orbit is taken to be the proper geodesic orbit around a Schwarzschild black hole, rather than a Keplerian orbit. The right panel shows the gravitational waveform associated with this orbit. For most of the orbit, there is little emitted radiation (the *zoom phase*), but when the small body passes near the black hole, it begins to *whirl*, emitting a highly structured burst of gravitational waves.

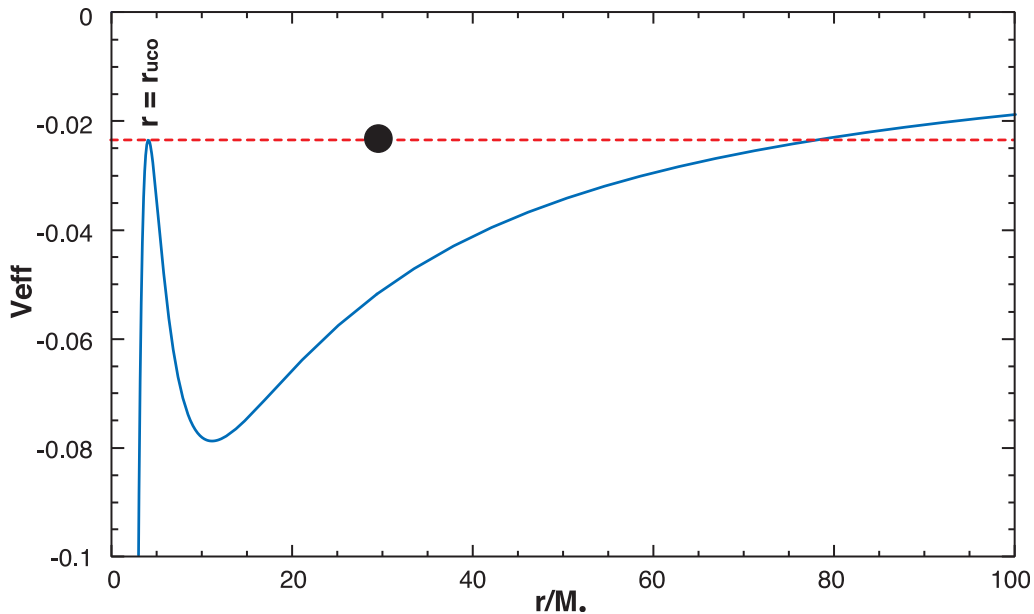


Figure 19: The effective potential around a Schwarzschild black hole, plotted versus the radial distance to the black hole (expressed in units of the black hole mass, M_{\bullet}). An EMRI moves on a bound orbit, moving between its turning points at the apocenter and pericenter. For the case shown, which exhibits the zoom whirl behaviour shown in Figure 18, the pericenter is very close to the inner most peak of the potential, located at $r = r_{uco}$, the radius of the inner *unstable circular orbit*.

In a very similar way (but much harder to illustrate), the oscillatory motion across the equatorial line shown by a whirling particle on an inclined orbit is simply an extreme form of relativistic precession. It is important to realize that during the whirling phase, the compact body is on a quasi-orbit which only appears roughly circular. The particle's radial position is ever decreasing during the first part of the whirling phase; even as the azimuthal phase (for instance) is accumulating rapidly, the radial distance is slowly decreasing as the particle approaches pericenter.

Because the whirling particles spend a significant number of quasi-orbits in the strongly curved region of the spacetime, near the black hole, the emitted gravitational waves will encode information from deep in the gravitational

potential of the black hole. As the stellar mass object traces out its complex trajectory, it samples the black hole potential at a variety of radii and angular orientations with respect to the black hole. The structure of the spacetime is fixed by the parameters which describe the black hole, such as the spin and mass. That information should, in principle, be encoded in the emitted gravitational radiation, and can be extracted from extended observations of the EMRI as it spirals into the supermassive black hole. The mapping of the black hole spacetime in this manner has come to be called *holiodesy*, in analogy with satellite geodesy which discerns the structure of the Earth's gravitational field by monitoring the orbits of satellites [141, 142].

Early work on the extraction of black hole maps [143, 144] showed that the multipolar information describing the central black hole's mass moments M_ℓ and mass-current moments S_ℓ is encoded in the waves. While it is known that the information is encoded in the emitted waves, no reliable demonstration has been completed to show *how* to extract the information out of the detected waveforms. The extraction of black hole parameters is intimately tied to the data analysis procedure used. Early studies to determine viable techniques to look for EMRIs have been based on template matching [78, 145]. These studies have largely focused on how to make template techniques computationally efficient enough to search over the enormous parameter space that zoom-whirl waveforms will occupy.

It is also possible that the EMRIs (particularly in light of the numbers shown in Table IV) will overlap to such a degree as to be *self-confused* – the total number visible to an observatory like LISA at any given time could produce a confusion limited background of astrophysical noise, similar to the predicted confusion background from the galactic binaries (see § 4.2)[146].

For a recent comprehensive review of EMRIs, readers are directed to [147].

4.5. Fundamental physics

Despite the obvious astrophysical motivations to observe the Universe in gravitational waves, a significant contribution of this emerging observational science will be in the realm of fundamental physics. For the first time, we will be able to probe the behaviour of gravity in dynamic and strong field regimes. For the most part, experimental probes of general relativity have been limited to weak field tests [148]. Tests of fundamental gravitational theory can take two basic forms: direct comparison of received gravitational wave signals to the predictions of general relativity, and bounding alternative theories of gravity by ascribing measurement errors to deviations from general relativity.

As a probe of strong field gravity, LISA will be a preeminent instrument, particularly in the face of many high signal to noise ratio sources, such as supermassive binary black holes and extreme mass ratio inspirals. Any detection of such sources can be a vehicle to answer a fundamental question about massive astrophysical systems: is the central massive object well described by the Kerr black holes of general relativity? Almost certainly any massive, compact object will exhibit some of the properties we associate with general relativity's black holes. For example, they will be axisymmetric and stationary (*i.e.*, appear identical at time t and $t + \Delta t$); if they were not, deviations from axisymmetry would have been bled away by emission of gravitational radiation. For any slowly rotating system, almost certainly the strength of the gravitational field itself will have made the body nearly spherical. This being the case, attempts to verify the character of astrophysical objects will have to resort to looking at other features which might discern them from traditional black holes. As an example, recent work has looked at the possibility of observing the gravitational wave evolution of EMRIs to distinguish central objects which might be boson stars instead of supermassive black holes of general relativity [149]. The trajectories around a boson star, which has no event horizon, will have a significantly different character than trajectories around a supermassive black hole. The differences can be understood by examining particle motion in the context of an effective potential of the boson star, similar to the effective potential interpretation for EMRI orbits around black holes described in §4.4.

When considering tests of the fundamental theory of gravity, the properties of the gravitational waves themselves can be exploited since they often differ between general relativity and alternative theories. In particular, the gravitational wave polarization states and the speed of propagation are key observational quantities which can be probed observationally.

In general relativity, gravitational waves can be decomposed (in the appropriate gauge, see [59] for extensive

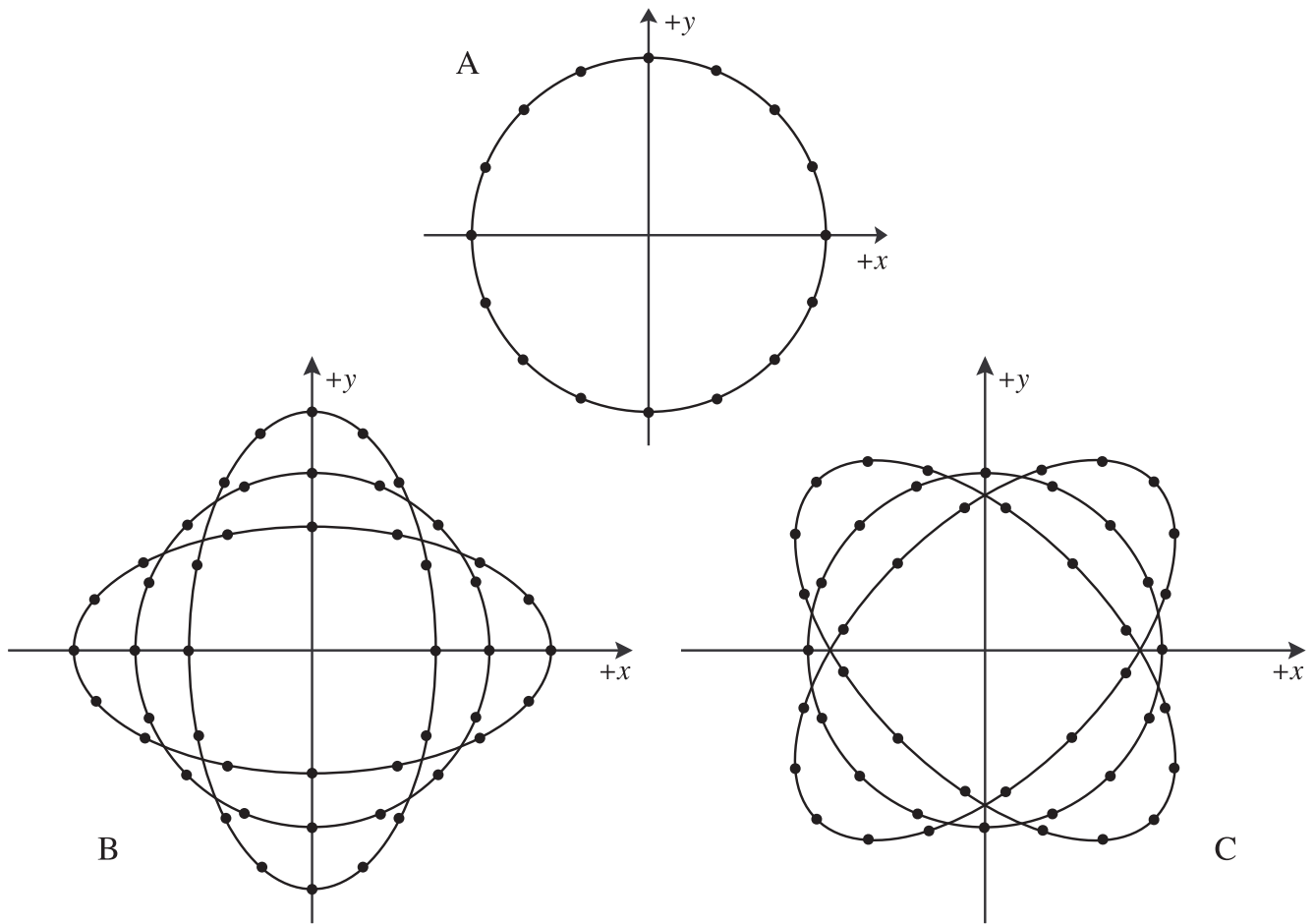


Figure 20: The polarization states in general relativity can be distinguished by using rings of test particles. Consider a circular ring of test particles in the $x - y$ plane as shown in (A). The passage of a $+$ polarized gravitational wave propagating out of the page (down the z -axis) will modulate the shape of the ring as shown in (B). Modulation of the ring shape due to passage of a \times polarized gravitational wave propagating down the z -axis is shown in (C). The multiple overlaying ellipses in (B) and (C) show the shape of the ring at times separated by half periods of the gravitational wave; the shape oscillates back and forth between the ellipses, through the undistorted circular shape of the original ring.

details) into two distinct polarization states, known $+$ (“plus”) and \times (“cross”) for the effect they have on the proper distances between individual members of an array of free test masses. A conventional pedagogical explanation of the differences between the two polarization states is shown in Figure 20, which illustrates the effect of a gravitational wave propagating out of the page and the resulting effect on a ring of free test particles. A general gravitational wave is simply a superposition of these two polarization states, and can be decomposed into two *polarization amplitudes*, h_+ and h_\times , which characterize the overall strength of each polarization in a received signal.

The basic principles of interferometric detector design are based on this heuristic picture; one can imagine the test masses at the ends of the LISA arms as being particles on the perimeter of this ring. When a gravitational wave passes by, the proper distance between the test masses changes as a consequence of this distortion. Because LISA’s arms are not orthogonal, any single LISA data stream will contain an admixture of both received gravitational wave polarization amplitudes, h_+ and h_\times , information which can be used to directly compare against the predictions of general relativity. Alternative theories of gravity can have a significantly different polarization structure, with as many as *six* different polarization states [150], and many studies have suggested that alternative theories can be tested by considering the response of interferometric observatories to polarization structure in gravitational wave signals [151–153].

Direct studies of using LISA observations to constrain alternative theories have considered the observation of inspiralling binaries [122, 154, 155] by LISA, and the bounds which can be derived by considering the *matched filtering* of signal data against template waveforms computed using general relativity.

The speed with which gravitational waves propagate can also be tested with gravitational wave observations and used to constrain alternative theories in comparison with general relativity which predicts that gravitational waves will propagate at the speed of light c . This question is often considered in terms of bounding the mass of the graviton, or the Compton wavelength which is related to the mass by $\lambda_c = h/m$, where h is the Planck constant and m is the graviton mass. Several different methods have been proposed to do this. If only gravitational wave information is considered, then a non-zero graviton mass will cause dispersion between waves of different frequency. This dispersion will influence the matching of templates for binary inspiral [156]. Another suggested method is to employ a *multi-messenger* approach, and compare gravitational wave and electromagnetic signals simultaneously received from the same source [157–159]. In this case, one compares the received gravitational wave phase with the phase of the electromagnetic light curve. If the graviton had a putative mass, the gravitational wave phase would lag behind the phase of the light curve when the waves reach Earth; the gravitational waves with frequency f propagated at a speed slower than c given by

$$v \simeq 1 - \frac{1}{2} \left(\frac{1}{\lambda_c f} \right)^2. \quad (49)$$

Most suggested experiments for constraining alternative theories are proposed as *null experiments*, where the assumption is that gravitational wave observations will validate the predictions of general relativity to the level of the LISA instrumental noise. The size of any deviations from general relativity can then be the size of the errors in the gravitational wave measurement and no larger. This maximum size for the deviation from general relativity then provides a natural constraint on the alternative theory.

4.6. Other possibilities

As with any new observational science, our expectations are that the Universe will be replete with unknown phenomena which we did not predict in advance. It is entirely possible that exotic astrophysical processes may produce significant amounts of gravitational radiation which will be detectable by observatories like LISA.

A final possible contributor in the low frequency gravitational wave band (not noted on Figure 11) is a *Cosmological Gravitational-wave Background* (CGB). Such a background is completely analogous to the electromagnetic Cosmic Microwave Background (CMB); it is generated as a consequence of early Universe physics, and encodes information about primordial density fluctuations and processes from a time well before the formation of large scale structure. An important characteristic of the CGB is that it originates at a higher redshift than the CMB, and if it were detectable (in any part of the gravitational wave spectrum) it would be an important probe to look beyond the recombination curtain. Given the current constraints on cosmological models from CMB experiments, it seems unlikely that a CGB from standard slow-roll inflation will be detectable by LISA. There are, however, other more exotic cosmological models which may still produce stochastic CGBs of detectable strength in the LISA band (for example, [160, 161], levels illustrated in [46]).

Another exciting prospect in gravitational wave astronomy is that observatories like LISA will be able to participate side by side with electromagnetic telescopes and astroparticle observatories as a major player in *multi-messenger astronomy*. This is currently a largely unexplored aspect of LISA science, though several early studies have begun to probe how coincident gravitational wave and electromagnetic observations can be used to enhance our understanding of the source systems LISA will observe [52, 157, 162, 163].

5. SUMMARY

LISA science is in a phase of rapid maturation on many frontiers, with strong advances currently being made in terms of what kind of astrophysical information will be encoded and extractable from LISA data, as well as rapid improvement in our understanding of data analysis techniques which will make the extraction of information from the LISA data possible.

More generally, gravitational wave astrophysics is rapidly evolving into a diverse multi-disciplinary field of research, bringing together traditional relativity theory, relativistic astrophysics, electromagnetic astronomy, engineering and high performance computing technology. This provides remarkable opportunities for young researchers entering the field, with important research questions still to be addressed in the areas of source characterization, source simulation, data analysis, and observatory design. The upcoming decade will be the years where the first generation of true gravitational wave astronomers will be trained – scientists who have never studied the Universe in the absence of gravitational wave data. The young researchers reading this document today will be in that generation, and LISA stands poised to be one of the primary instruments which will open this new window on the Universe.

Acknowledgments

SLL acknowledges support at Penn State from the Center for Gravitational Wave Physics, funded by the NSF under cooperative agreement PHY 01-14375, and from NASA award NNG05GF71G.

References

- [1] A. Abramovici *et al.*, 1992, *Science*, **256**, 325.
- [2] J. Hough, et al., “GEO 600: Current status and some aspects of the design”, in *Proceedings of Conference on Gravitational Wave Detection*, K. Tsubono, M. Fujimoto, M.K., and K. Kuroda eds., Universal Academy Press, Tokyo (1997).
- [3] C. Bradaschia *et al.*, Nucl. Instrum. & Methods A **289**, 518 (1990); for a more recent update see A. Brillet, “VIRGO Status Report November 1997”, in *Second Edoardo Amaldi Conference on Gravitational Waves*, E. Coccia, G. Veneziano and G. Pizzella eds., World Scientific, Singapore (1998).
- [4] G. Pizzella, 1997, *Class. Quant. Grav.* **14**, 1481
- [5] E. Coccia, 2003, *Class. Quant. Grav.* **20**, S135
- [6] F. B. Estabrook and H. D. Wahlquist, 1975, *Gen. Rel. Grav.* **6**, 439.
- [7] R. W. Hellings, 1978, *Phys. Rev. D* **17**, 3158.
- [8] R. W. Hellings, 1981, *Phys. Rev. D* **23**, 832.
- [9] R. W. Hellings and G. S. Downs, 1983, *Astrophys. J.* **265**, L39.
- [10] V. M. Kaspi, J. H. Taylor, and M. F. Ryba, 1994, *Astrophys. J.* **428**, 713.
- [11] W. Hu and M. White, 1997, *New Astron.* **2**, 323
- [12] K. S. Thorne, “Gravitational Radiation”, in *300 Years of Gravitation*, W. Israel and S. W. Hawking eds., pgs. 330-458 (1987).
- [13] J. E. Faller, P. L. Bender, J. L. Hall, D. Hils, and M. A. Vincent, *Space antenna for gravitational wave astronomy*, in “Proceedings of the Colloquium on Kilometric Optical Arrays in Space”, SP-226, ESA (1985) .
- [14] R. W. Hellings *et al.* *SAGITTARIUS Mission Concept Study*, JPL Engineering Memorandum 314-569 (1993).
- [15] R. W. Hellings *et al.*, *Orbiting Medium Explorer for Gravitational Astrophysics (OMEGA)*, proposal to NASA Medium Explorer program, (1998) (unpublished).
- [16] J. B. Hartle *et al.*, *Gravitational Physics*, National Academy Press, Washington DC (1999).
- [17] C. F. McKee *et al.*, *Astronomy and Astrophysics in the New Millennium*, National Academy Press, Washington DC (2000).

- [18] E. S. Phinney *et al.*, *Beyond Einstein: from the Big Bang to black holes (Structure and Evolution of the Universe Roadmap)*, NP-2002-10-510-GSFC (2003).
- [19] For more information on *Constellation-X*, visit their website at <http://constellation.gsfc.nasa.gov/>.
- [20] P. Bender *et al.*, *LISA Pre-Phase A Report*, Max-Planck-Institut für Quantenoptik, Garching, second edition, (1998).
- [21] T. Edwards *et al.*, *LISA: Study of the Laser Interferometer Space Antenna: Final Technical Report (FTR)*, Dornier Satellitensysteme GmbH, DSS Report No. LI-RP-DS-009 (2000).
- [22] *LISA: Laser Interferometer Space Antenna: A cornerstone mission for the observation of gravitational waves, System and Technology Study Report (STS)*, ESA-SCI(2000)11 (2000).
- [23] Shane L. Larson, *Online Sensitivity Curve Generator*, located at <http://www.srl.caltech.edu/~shane/sensitivity/>; based on S. L. Larson, W. A. Hiscock & R. W. Hellings, 2000, Phys. Rev. D, **62**, 062001.
- [24] S. V. Dhurandhar *et al.*, 2005, Class. Quant. Grav., **22**, 481.
- [25] S. P. Hughes, in "Guidance and Control", Proceedings of the 25th Annual AAS Rocky Mountain Guidance and Control Conference, R. D. Culp and S. D. Jolly eds., pgs. 61-78 (2002).
- [26] L. J. Rubbo, N. J. Cornish and O. Poujade, 2004, Phys. Rev. D, **69**, 082003.
- [27] F. B. Estabrook, M. Tinto and J. W. Armstrong, 2000, Phys. Rev. D, **62**, 042002.
- [28] J. W. Armstrong, F. B. Estabrook and M. Tinto, Astrophys. J., 1999, **527**, 814.
- [29] M. Vallisneri, 2005, Phys. Rev. D, **72**, 042003.
- [30] N. J. Cornish and R. W. Hellings, 2003, Class. Quant. Grav., **20**, 4851.
- [31] D. A. Shaddock, M. Tinto, F. B. Estabrook and J. W. Armstrong, 2003, Phys. Rev. D, **68**, 061303.
- [32] T. A. Prince, M. Tinto, S. L. Larson and J. W. Armstrong, 2002, Phys. Rev. D, **66**, 122002.
- [33] D. A. Shaddock, 2004, Phys. Rev. D, **69**, 022001.
- [34] M. Tinto, F. B. Estabrook and J. W. Armstrong, 2004, Phys. Rev. D, **69**, 082001.
- [35] Michele Vallisneri, *Synthetic LISA*, located at <http://www.vallis.org/syntheticlisa/> based on M. Vallisneri, 2005, Phys. Rev. D, **71**, 022001.
- [36] *The LISA Simulator*, located at <http://physics.montana.edu/lisa/>; based on L. J. Rubbo, N. J. Cornish and O. Poujade, 2004, Phys. Rev. D, **69**, 082003
- [37] M. Tinto, 1998, Phys. Rev. D **58**, 102001.
- [38] M. Tinto and S. V. Dhurandhar, 2005, Living Rev. Relativity **8**,4. URL (cited on 23 September 2005): <http://www.livingreviews.org/lrr-2005-4>
- [39] M. Tinto, J. W. Armstrong and F. B. Estabrook, 2000, Phys. Rev. D, **63**, 021101(R).
- [40] C. Hogan and P. Bender, 2001, Phys. Rev. D **64**, 062002.
- [41] M. Tinto and S. L. Larson, 2004, Phys. Rev. D **70**, 062002.
- [42] M. Tinto and S. L. Larson, 2005, Class. Quant. Grav., **22**, 531.
- [43] Y. Gursel and M. Tinto, 1989, Phys. Rev. D, **40**, 3884.
- [44] S. L. Larson, W. A. Hiscock and R. W. Hellings, 2000, Phys. Rev. D **62**, 062001.
- [45] S. L. Larson, R. W. Hellings and W. A. Hiscock, 2002, Phys. Rev. D **66**, 062001.
- [46] N. J. Cornish and S. L. Larson, 2001, Class. Quant. Grav., **18**, 4277.
- [47] N. J. Cornish and L. J. Rubbo, 2003, Phys. Rev. D **67**, 022001.
- [48] C. Cutler, 1998, Phys. Rev. D **57**, 7089.
- [49] Footnote [44] of L. S. Finn and K. S. Thorne, 2000, Phys. Rev. D **62**, 124021.
- [50] A. Vecchio and E. D. L. Wickham, 2004, Phys. Rev. D **70**, 082002.
- [51] E. Flanagan and S. Hughes, 1998, Phys. Rev. D, **57**, 4535
- [52] B. Kocsis *et al.*, 2005, astro-ph/0505394; accepted for publication in Astrophys. J.
- [53] P. C. Peters and J. Mathews, 1963, Phys. Rev., **131**, 435.
- [54] P. C. Peters, 1964, Phys. Rev., **136**, 4B 1224.
- [55] J. R. Gair, D. Kenefick and S. L. Larson, 2005, Phys. Rev. D **72**, 084009
- [56] H. D. Wahlquist, 1987, Gen. Relativ. Gravit., **19**, 1101.

- [57] L. Blanchet, B. R. Iyer, C. M. Will and A. G. Wiseman, 1996, *Class. Quant. Grav.*, **13**, 575.
- [58] T. A. Moore, and R. W. Hellings, 2002, *Phys. Rev. D*, **65**, 062001.
- [59] C. Misner, K. Thorne and J. Wheeler, *Gravitation*, W. H. Freeman (1973).
- [60] A. Einstein, 1918, *Sitzungsber. Preuss. Akad. Wiss., Phys. Math. Kl.*, 154
- [61] A. Vecchio, 2004, *Phys. Rev. D*, **70**, 042001
- [62] M. Benacquista, 1999, *Astrophys. J.* **520**, 233
- [63] *The LISA Calculator*, located at <http://www.physics.montana.edu/LISA/lisacalculator/>, N. J. Cornish and J. C. Crowder.
- [64] C. Culter and K. Thorne, *An overview of gravitational-wave sources*, to appear in Proceedings of GR16; gr-qc/0204090
- [65] D. Hils, P. L. Bender and R. F. Webbink, 1990, *Astrophys. J.*, **360**, 75; (erratum) 1991, *Astrophys. J.*, **369**, 271
- [66] P. L. Bender and D. Hils, 1997, *Class. Quant. Grav.*, **14**, 1439.
- [67] D. Hils and P. L. Bender, 2000, *Astrophys. J.*, **537**, 334.
- [68] G. Nelemans *et al.*, 2001, *Astron. Astrophys.*, **365**, 491.
- [69] G. Nelemans *et al.*, 2001, *Astron. Astrophys.*, **368**, 939.
- [70] M. Benacquista, J. DeGoes and D. Lunder, 2004, *Class. Quant. Grav.*, **21**, S509.
- [71] J. A. Edlund *et al.*, 2005, *Phys. Rev. D* **71**, 122003.
- [72] E. Robinson and A. Shafter, 1987, *Astrophys. J.*, **322**, 296
- [73] T. Marsh, V. Dhillon and S. Duck, 1995, *Mon. Not. Roy. Astr. Soc.*, **275**, 828
- [74] T. Marsh, 1995, *Mon. Not. Roy. Astr. Soc.*, **275**, L1
- [75] C. Karl *et al.*, 2003, *Astron. Astrophys.*, **410**, 663
- [76] G. Nelemans *et al.*, 2005, *Astron. Astrophys.*, **440**, 1087
- [77] S. A. Hughes, 2002, *Mon. Not. Roy. Astr. Soc.*, **331**, 805.
- [78] J. R. Gair *et al.*, 2004, *Class. Quant. Grav.*, **21**, 1595
- [79] N. Cornish, *Gravitational wave confusion noise*; gr-qc/0304020 (2003).
- [80] C. Hellier, *Cataclysmic variable stars*, Springer-Praxis, London (2001).
- [81] National Space Science Data Center, <http://nssdc.gsfc.nasa.gov/>.
- [82] HEASARC Data Archive, <http://heasarc.gsfc.nasa.gov/docs/archive.html>
- [83] M. Meliani, J. de Araujo and O. Aguiar, 2000, *Astron. Astrophys.* **358**, 417
- [84] S. F. Anderson *et al.*, 2005, *Astron. J.* **130**, 2230
- [85] N. J. Cornish and S. L. Larson, 2003, *Phys. Rev. D* **67**, 103001
- [86] A. Krolak and M. Tinto, in *Proceedings of the 10th Marcel Grossman Meeting*; gr-qc/0302013
- [87] N. Seto, 2004, *Phys. Rev. D* **69**, 123005.
- [88] N. Seto and A. Cooray, 2004, *Phys. Rev. D* **70**, 123005
- [89] W. A. Hiscock, S. L. Larson, J. R. Routzahn and B. Kulick, 2000, *Astrophys. J.*, **540**, L5
- [90] W. A. Hiscock, 1998, *Astrophys. J.*, **509**, L101
- [91] K. Ioka, T. Tanaka and T. Nakamura, 2000, *Astrophys. J.*, **528**, 51
- [92] A. J. Farmer and E. S. Phinney, 2003, *Mon. Not. Roy. Astr. Soc.*, **346**, 1197
- [93] X. Fan *et al.* (SDSS Collaboration), 2000, *Astron. J.* **120**, 1167
- [94] D. Stern *et al.*, 2000, *Astrophys. J.* **533**, L75
- [95] W. Zheng *et al.* (SDSS Collaboration), 2000, *Astron. J.* **120**, 1607
- [96] J. Kormendy and D. Richstone, 1995, *Ann. Rev. Astron. Astrophys.* **33**, 581
- [97] J. Magorrian *et al.*, 1998, *Astron. J.* **115**, 2285
- [98] K. Gebhardt *et al.*, 2000, *Astrophys. J.* **539**, L13
- [99] L. Ferrarese and D. Merritt, 2000, *Astrophys. J.* **539**, L9
- [100] J. Kormendy and K. Gebhardt, in *Proceedings of the 20th Texas Symposium on Relativistic Astrophysics*, H. Martel and J. C. Wheeler eds., pgs. 363-381 (2002).

- [101] L. Ferrarese and D. Merritt, 2000, *Astrophys. J.* **539**, L9
- [102] S. Tremaine *et al.*, 2002, *Astrophys. J.* **574**, 740
- [103] K. Gebhardt, R. M. Rich and L. C. Ho, 2002, *Astrophys. J.* **578**, L41
- [104] R. P. van der Marel *et al.*, 2002, *Astron. J.* **124**, 3255
- [105] J. Gerssen *et al.*, 2002, *Astron. J.* **124**, 3270
- [106] J. Gerssen *et al.*, 2003, *Astron. J.* **125**, 376
- [107] K. Gebhardt, R. M. Rich and L. C. Ho, astro-ph/0508251; accepted for publication in *Astrophys. J.*
- [108] M. C. Aller and D. Richstone, 2002, *Astron. J.* **124**, 3035
- [109] K. Menou, Z. Haiman and V. Narayanan, 2001, *Astrophys. J.*, **558**, 535
- [110] A. Sessana *et al.*, 2005, *Astrophys. J.*, **623**, 23
- [111] K. J. Rhook and J. S. B. Wyithe, 2005, *Mon. Not. Roy. Astr. Soc.*, **361**, 1145.
- [112] M. Haehnelt, 1994, *Mon. Not. Roy. Astr. Soc.*, **269**, 199.
- [113] M. Volonteri, F. Haardt and P. Madau, 2003, *Astrophys. J.*, **582**, 559
- [114] M. Volonteri, P. Madau and F. Haardt, 2003, *Astrophys. J.*, **593**, 661
- [115] K. Menou, Z. Haiman and V. Narayanan, 2001, *Astrophys. J.*, **558**, 535
- [116] S. Hughes, 2002, *Mon. Not. Roy. Astr. Soc.*, **331**, 805.
- [117] P. Laguna, in "100 Years of Relativity - Spacetime Structure: Einstein and Beyond", A. Ashtekar ed., World Scientific (2005).
- [118] S. Shapiro, in "The Next Chapter in Einstein's Legacy", Proceedings of YKIS 2005, M. Sasaki, J. Soda and T. Tanaka eds., in *Progress of Theoretical Physics Suppl.*, in press (2006)
- [119] B. Bruegmann, W. Tichy and N. Jansen, 2004, *Phys. Rev. Lett.* **92**, 211101
- [120] F. Pretorius, 2005, *Phys. Rev. Lett.* **95**, 121101
- [121] E. Berti, A. Buonanno and C. Will, 2005, *Class. Quant. Grav.*, **22**, S943
- [122] E. Berti, A. Buonanno and C. Will, 2005, *Phys. Rev. D*, **71**, 084025
- [123] S. Hughes and R. Blandford, 2003, *Astrophys. J.*, **585**, L101
- [124] For example, see Ned Wright's *Online Javascript Cosmology Calculator*, located at: <http://www.astro.ucla.edu/~wright/CosmoCalc.html>
- [125] K. Kokkotas and B. Schmidt, 1999, *Living Rev. Relativity* **2**,2. URL (cited on 23 September 2005): <http://www.livingreviews.org/lrr-1999-2>
- [126] S. Sigurdsson and M. Rees, 1997, *Mon. Not. Roy. Astr. Soc.*, **284**, 318
- [127] S. Aarseth, 1999, *Proc. Astr. Soc. Pac.* **111**, 1333
- [128] S. Aarseth, 1999, *Cel. Mech. Dyn. Astr.* **73**, 127
- [129] R. Spurzem, 1999, *J. Comp. Appl. Math.* **109**, 407
- [130] M. Freitag and W. Benz, 2001, *Astron. Astrophys.*, **375**, 711
- [131] M. Freitag and W. Benz, 2002, *Astron. Astrophys.*, **394**, 345
- [132] M. Freitag, 2001, *Class. Quant. Grav.*, **18**, 4033
- [133] M. Hénon, in *Dynamical structure and evolution of stellar systems*, Lectures of the 3rd Advanced Course of the Swiss Society for Astronomy and Astrophysics, L. Martinet and M. Mayor eds, pgs. 183-260 (1973).
- [134] P. Ivanov, 2002, *Mon. Not. Roy. Astr. Soc.*, **336**, 373
- [135] D. Hils and P. Bender, 1995, *Astrophys. J.*, **445**, L7
- [136] R. Schödel *et al.*, 2003, *Astrophys. J.*, **596**, 1015
- [137] A. Ghez *et al.*, 2005, *Astrophys. J.*, **620**, 744
- [138] R. Schödel *et al.*, 2002, *Nature* **419**, 694
- [139] M. Freitag, 2003, *Astrophys. J.*, **583**, L21
- [140] K. Glampedakis and D. Kennefick, 2002, *Phys. Rev. D* **66**, 044002
- [141] J. Wahr, 2004, *Geophys. Res. Lett.* **31**, L11501
- [142] J. Chen, 2004, *Geophys. Res. Lett.* **31**, L22607
- [143] F. Ryan, 1995, *Phys. Rev. D* **52**, 5707

- [144] F. Ryan, 1997, Phys. Rev. D **56**, 1845
- [145] L. Barack and C. Cutler, 2004, Phys. Rev. D **69**, 082005
- [146] L. Barack and C. Cutler, 2004, Phys. Rev. D **70**, 122002
- [147] K. Glampedakis, 2005, Class. Quant. Grav. **22**, S605
- [148] C. Will, 2001, Living Rev. Relativity **4**,4. URL (cited on 23 September 2005): <http://www.livingreviews.org/lrr-2001-4>
- [149] M. Kesden, J. Gair and M. Kamionkowski, 2005, Phys. Rev. D **71**, 044015
- [150] C. M. Will, *Theory and Experiment in Gravitational Physics*, 2nd Ed., Cambridge University Press (1993).
- [151] M. Brunetti *et al.*, 1999, Phys. Rev. D **59**, 044027
- [152] M. Maggiore and A. Nicolis, 2000, Phys. Rev. D **62**, 024004
- [153] K. Nakao *et al.*, 2001, Phys. Rev. D **63**, 082001
- [154] P. Scharre and C. Will, 2002, Phys. Rev. D **65**, 042002
- [155] C. Will and N. Yunes, 2004, Class. Quant. Grav. **21**, 4367
- [156] C. M. Will, 1998, Phys. Rev. D **57**, 2061
- [157] S. L. Larson and W. A. Hiscock, 2000, Phys. Rev. D **61**, 104008
- [158] C. Cutler, W. A. Hiscock and S. L. Larson, 2003, Phys. Rev. D **67**, 024015
- [159] A. Cooray and N. Seto, 2004, Phys. Rev. D **69**, 103502
- [160] C. Hogan, 2000, Phys. Rev. Lett. **85**, 2044
- [161] R. Riazuelo and J-P. Uzan, 2000, Phys. Rev. D **62**, 083506
- [162] M. Milosavljevic and E. S. Phinney, 2005, Astrophys. J., **622**, L93
- [163] A. Cooray, A. J. Farmer and N. Seto, 2004, Astrophys. J., **601**, L47